HEDL-TME 71-110

AUGUST 1971



# THE SIMULATION OF SHORT-TERM ANNEALING OF DISPLACEMENT CASCADES IN $\gamma$-IRON

HANFORD ENGINEERING DEVELOPMENT LABORATORY

UNITED STATES ATOMIC ENERGY COMMISSION

Operated by

WADCO CORPORATION

CONTRACT AT(45-1)-2170

---

# THE SIMULATION OF SHORT-TERM ANNEALING OF DISPLACEMENT CASCADES IN $\gamma$-IRON

By

D. G. Doran
WADCO Corp., Hanford Engineering Development Laboratory
Richland, Washington

and

R. A. Burnett
Battelle, Pacific Northwest Laboratories
Richland, Washington



Hanford Engineering Development Laboratory
Richland, Washington, operated by WADCO Corporation, a subsidiary of Westinghouse Electric Corporation for the United States Atomic Energy Commission under Contract No. AT(45-1)-2170

This paper covers work performed by Battelle-Northwest under AEC Contract No. AT (45-1)-1820 and WADCO Corporation under AEC Contract No. AT(45-1)-2170.

# THE SIMULATION OF SHORT-TERM ANNEALING OF DISPLACEMENT CASCADES IN $\gamma$-IRON

By

D. G. Doran
WADCO Corp., Hanford Engineering Development Laboratory
Richland, Washington

and

R. A. Burnett
Battelle, Pacific Northwest Laboratories
Richland, Washington

## ABSTRACT

An important source of damage to a solid exposed to high energy neutrons (or ions) is the displacement of atoms from normal lattice sites. In a fast reactor, energies of tens of keV may be transferred to an atom and thus initiate a displacement cascade consisting of a localized high density of interstitials and vacancies. These defects will subsequently interact with one another to form clusters and to reduce their density by mutual annihilation. This short-term annealing of an isolated cascade has been simulated at high and low temperatures with a small computer using an atomic model of $\gamma$-iron based on the work of Johnson. The input cascades are due to Beeler. Results were obtained with both large (104 sites) and small (32 sites) annihilation regions. The former results in about one-half the residual defects of the latter, and a smaller fraction of clustered defects. Cluster size distributions and several examples of spatial distributions are given. Randomizing the spatial distribution of defects in a typical cascade geometry is found to diminish vacancy clustering and enhance interstitial clustering.

CONTENTS

# FIGURES

FIGURES (Cont'd)

# TABLES

# 1 INTRODUCTION

An important source of damage to a solid exposed to high energy neutrons (or ions) is the displacement of atoms from normal lattice sites. In a fast reactor, energies of tens of keV may be transferred to the primary knock-on atom (PKA), producing in medium and high atomic weight materials a displacement cascade comprising a localized high density of vacancies and interstitials. These defects will subsequently interact with one another to produce clusters and to reduce their density by mutual annihilation--a process called short-term annealing in the present context.

The objective of this work was to determine by computer simulation the defect clustering characteristics of $\gamma$-iron, a stand-in for the stainless steel used in fast reactors. Both high and low temperatures were studied. Also investigated was the influence of the cascade formation process on the short-term annealing characteristics of a given density of defects. This was examined with a "randomized cascade" created by introducing defects at randomly selected positions within a typical cascade volume.

In a previous paper[1] the annealing simulation work initiated by Beeler and Besco[2,3] was extended and applied to a description of short-term annealing of cascades in $\alpha$-iron (bcc lattice). This paper is concerned with a new program to simulate short-term annealing in an fcc lattice, and its application to cascades produced by Beeler.[2] The new code employs a model for $\gamma$-iron based on the work of R.A. Johnson.[4] Beeler used a copper model in his fcc work, but there is no basis for distinguishing between copper and $\gamma$-iron at the present level of sophistication.

The results obtained in this study and in related work are of importance to the LMFBR program in at least two applied areas, as well as contributing to the understanding of the processes by which fast neutrons interact with solids. These areas are (1) parameter definition in kinetic descriptions of damage processes, and (2) the dependence of damage on neutron spectra. The implications of the annealing simulation work in these areas will be the subject of a separate report.

## 2 COMPUTATIONAL DETAILS

### 2.1 The Machine

A hybrid computer facility* consisting of a Beckman 2133 analog computer and a PDP-7 digital computer (8K memory) was used in this work. Actually, a random noise generator used to generate random numbers was the only contribution from the analog side. The digital program, HAPFCC (Hybrid Anneal Program--FCC), was written in assembly language.

The primary reason for using the small computer is the high level of man-machine interaction it provides--a significant consideration because the annealing runs are open-ended. Parameters can be changed through teletype entry at the beginning of a run, and several options can be exercised through console switches to control a run in progress. In addition, the program runs faster than an equivalent FORTRAN program on the available big machine (a UNIVAC 1108) and the charge rate is much lower on the small machine.

Initial defect distributions were read into the computer from punched cards, and intermediate and final distributions were stored on magnetic tape. Both tabular and graphic outputs were recorded with an electrostatic line printer.

HAPFCC can handle a maximum of 432 defect pairs within that portion of the 8K memory not required for program instructions. This was sufficient to handle the largest cascades presently available but was a minor limitation in studying randomized cascades, as will be apparent below.

### 2.2 Program Description and Operation

The annealing program, a correlated random walk on an fcc lattice, is defined by the following: the identity of mobile defects, jump vectors and jump probabilities of mobile defects, definition of correlated jumps and their relative jump probabilities, clustering criteria, and annihilation criteria.

During each time step, each member of each migrating cluster (of the appropriate type) is considered once, in random order, for a jump. A permissible jump vector is chosen at random, possible correlations sought, and the jump performed or not performed according to the assigned probability through selection of another random number. If a jump results, an examination is made for possible clustering or annihilation.

---

* Operated by Computers and Control Section of Battelle-Northwest.

High temperature (nominally 800° K) operation was characterized by two successive stages because of the large difference in mobilities of vacancies and interstitials. During the high temperature-interstitial stage, the much slower vacancies were ignored except as they participated in annihilation of migrating interstitials. During the subsequent vacancy stage, interstitials were immobilized to conserve computer time. This procedure poses no problem at the beginning of the vacancy stage because only immobile interstitial complexes remain in the vicinity of the vacancies. Ultimately, however, some of the by-products of annihilation are mobile interstitials. An effort was made to determine the behavior of the newly created mobile interstitials (see Section 4.1.1).

The time step in the high temperature-interstitial stage was such that the uncorrelated jump probability of the most mobile defect ($I_1$)* was 0.5; the correlated probability was unity. The vacancy stage time step was chosen so that the highly mobile $V_2$ jumped once per step.**

It was found that 1000 to 2000 time steps in a given stage generally reduced the frequency of defect interactions to the order of one per 500 steps.

Low temperature (nominally 300° K) operation was characterized by permitting only interstitials to migrate. The time step was chosen to be consistent with the high temperature case, such that the uncorrelated jump probability of an $I_1$ was 0.14; the correlated probability was unity. The jump probabilities of di- and tri-interstitials were so small as to be negligible for the 1000 to 2000 time step duration of the runs. This condition should prevail--and hence this model is considered reasonable--to about 500° K.

Ten 20 keV and ten 5 keV cascades were selected for processing. These cascades are a subset of those which provided the cluster size distributions of reference 2. Those distributions were obtained by Beeler from a computer program CLUSTER which applied clustering criteria to the output of the CASCADE program. For the present work, only the CASCADE outputs were utilized. Inherent in them is the recombination of all related interstitial-vacancy pairs (unrelated pairs are not recognized) separated by less than $\sqrt{5}$ half-lattice units (hlu);*** the interstitials are at octahedral sites. The initial operation

---

* The symbols $I_n$ and $V_n$ designate interstitial and vacancy clusters, respectively, of size n.

** The relative jump probabilities should be reasonably representative of the temperature range 600-1000° K.

***1 hlu = 1.823 Å for $\gamma$-iron.

of the HAPFCC program is to assign each octahedral interstitial to a randomly chosen neighboring fcc site and to assign to it an orientation along a randomly chosen major axis.

The spatial distribution of defects in a displacement cascade is a rather special one in which a vacancy-rich central region is surrounded by an interstitial-rich peripheral region. An effort was made to determine how strongly this configuration influences the cluster size distribution. The geometrical configuration of one 20 keV cascade (No. 2076) was determined by computer-plotting the defects plane by plane; a simplified representation of the contribution from each plane was used (see Figure 1). A library of alternating interstitial and vacancy sites was prepared by randomly selecting sites within the geometrical figure that resulted from stacking the slabs (total volume of ~15,000 $hlu^3$). A "randomized cascade" was created by selecting 400+ defects of each type from this library, eliminating unlike defects which were first or second neighbors (as was done with 20 keV cascades), adding more defects, etc., until the desired number of defects was reached. This iterative procedure was necessary because of the program limitation of 432 defect pairs. Only two iterations were required to reach the goal of ~250 pairs, the number of defects in a 20 keV displacement cascade after first and second neighbor unlike defects have recombined.

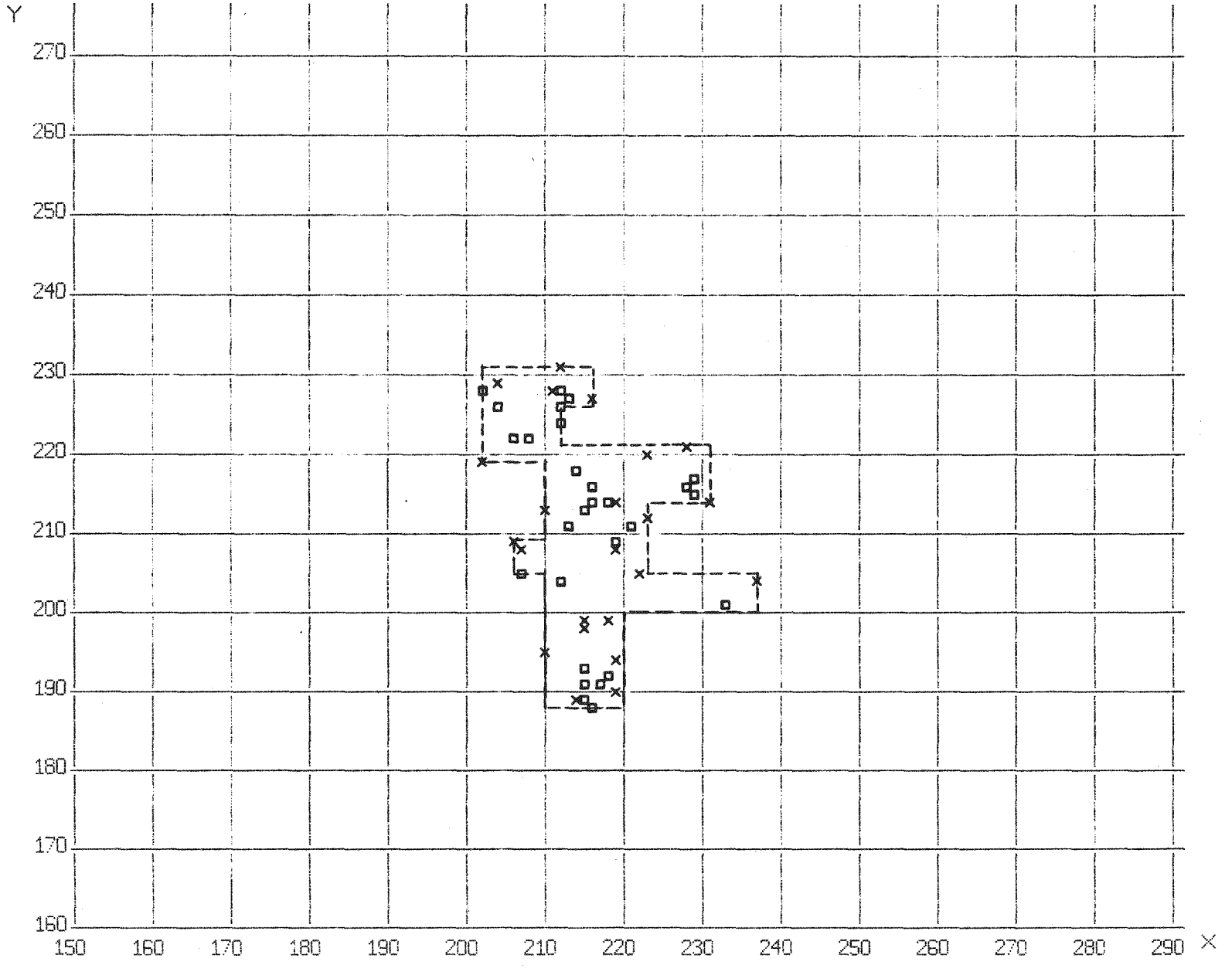


Figure 1. A single plane through the pre-anneal configuration of a 20 keV cascade (No. 2076), and its representation used in defining a randomized cascade. Squares and Xs are vacancies and interstitials, respectively. Dimension is the half-lattice constant.

## 3 THE $\gamma$-IRON MODEL

The model is based on Johnson's[4] simulation of point defects and small clusters in $\gamma$-iron. The activation energies found by him lead to the following hierarchy of the mobile defects included in this work, starting with the most mobile: $I_1$, $I_2$, $I_3$, $V_2$, $V_3$, and $V_1$. The large gap in mobility between the slowest moving interstitial ($I_3$) and the fastest moving vacancy ($V_2$), even at high temperatures, led to separate interstitial and vacancy annealing stages in HAPFCC.

Johnson found interstitial behavior to be very complex and his treatment is incomplete. Even so, we have not attempted to incorporate all of his results but have tried to retain their essence.

The stable $I_1$ is, following Johnson, the <100> split interstitial. In migrating, an x-oriented $I_1$ can jump to 8 possible first neighbor sites such that $\Delta x = \pm 1$; e.g., a jump in the x-z plane corresponds to $\Delta y = 0$, $\Delta z = \pm 1$ and a new (z) orientation. The motion of an $I_1$ that is within a 4th neighbor separation of another $I_1$ is correlated such that the jump probability is unity toward the formation of the stable $I_2$ (see Figure 2-a). If relative orientations preclude stable $I_2$ formation, the jump probability for increasing the separation is unity. If an $I_1$ is within a 4th neighbor separation of a clustered interstitial or two or more interstitials (clustered or single), a jump to decrease the total separation has a probability of unity, while a jump to increase the total separation is not permitted.

In addition, a longer ranged correlation for single interstitials can be used; viz., a jump toward another interstitial has probability $\alpha$ if the proposed jump site is a 4th or nearer neighbor of the other interstitial (in the present work, $\alpha = 1$).

A first neighbor bond constitutes clustering. The $I_2$ configuration is always two parallel interstitials, their common orientation being perpendicular to a line joining their centers (see Figure 2-a). The $I_2$ migrates only in the plane perpendicular to its orientation, with an uncorrelated jump probability of 0.12 relative to the $I_1$. The 4th neighbor correlation scheme above applies to each member of an $I_2$.

The $I_3$ is permitted to exist in two $I_3$ (112)* configurations (see Figure 2-b, c). Since the $I_2$ is already in the most stable configuration, the third interstitial can take up one of four sites in the plane perpendicular to the orientation of the $I_2$. Furthermore, it can be

*Indicates 3 bonds, 2 of which are 1st neighbor bonds and one of which is a 2nd neighbor bond.

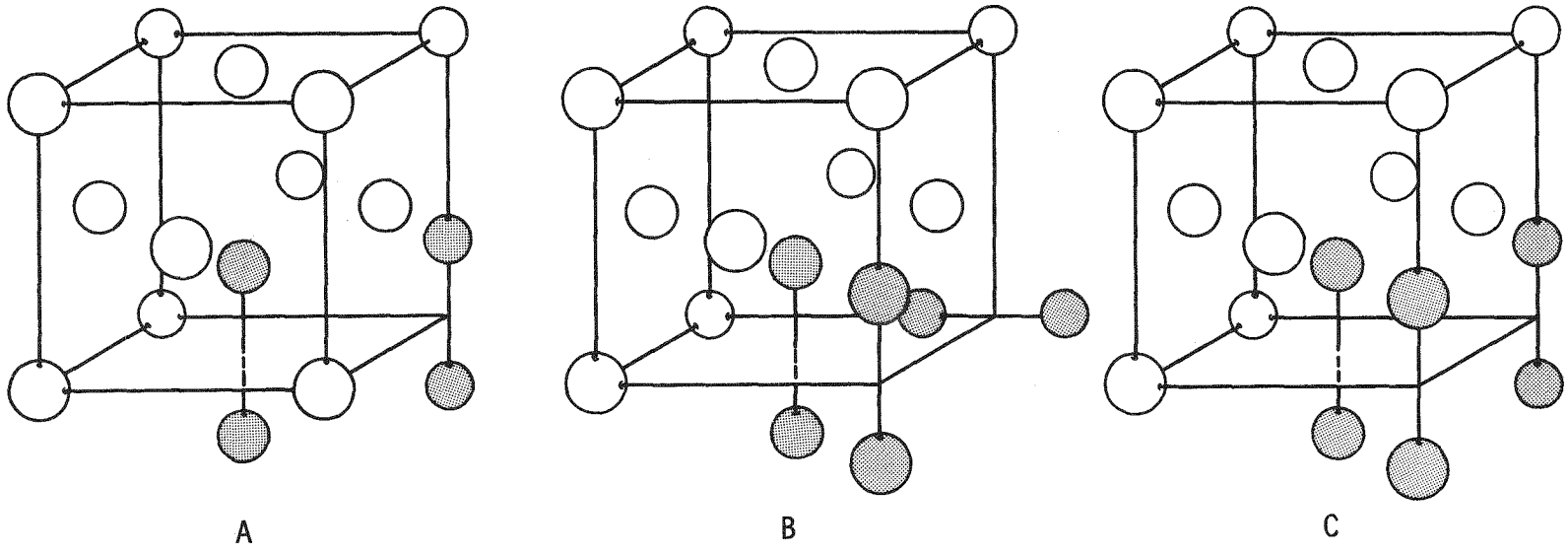


Figure 2. Interstitial configurations studied by Johnson.[4] (a) The stable $I_2$. (b) The most stable $I_3$. (c) An alternative form of $I_3$.

oriented parallel to the $I_2$ or lie in the plane of the $I_3$; the latter (Figure 2-b) was found by Johnson to be the lowest energy configuration. Migration of the "parallel" $I_3$ is confined to the plane of the defect, but the most stable $I_3$ can migrate in three dimensions. Jump probabilities relative to the $I_1$ are 0.011, but the stable form can reorient with a relative probability of 1.0.

An interstitial cluster of size 4 or larger is considered immobile and no orientation information of its members is retained. Hence the morphology of the cluster has no significance. No dissociation of clusters is permitted.

Mobile species of vacancies are confined to $V_1$, $V_2$, $V_3$, and $V_4$. Either member of the $V_2$, a nearest neighbor pair, can jump to one of the 4 first neighbor sites in the plane bisecting their bond. Dissociation of the $V_2$, or any vacancy cluster, is not permitted.

The stable forms of the $V_3$ and $V_4$ are the triangle, $V_3(111)$, and the tetrahedron, $V_4$ (111111), and these configurations are immediately imposed when such clusters form. The $V_3$ can reorient by shifting the associated vacancy among the 4 sites of the tetrahedron; the reorientation frequency is equivalent to the $V_2$ jump frequency. The $V_3$ migrates with either a $V_3$ (112) or $V_3$ (113) intermediate state. The $V_4$ migrates effectively one half-lattice unit in a <100> direction, undergoing simultaneously a 90° rotation. Higher order vacancy clusters are considered immobile.

Vacancy correlations, limited to short range, are summarized in Table 1. Some of the associated activation energies are based on work by the authors using Johnson's $\gamma$-iron potential in the code DEFECT.* Relative jump probabilities are, of course, dependent on the temperature.

An important but inadequately defined parameter, the annihilation region (AR), describes the attraction of a vacancy for an interstitial and the resulting annihilation of both defects. The AR is a set of sites relative to the position of the interstitial and dependent on its orientation, such that, if a vacancy occupies one of the sites, the interstitial and vacancy are considered to suffer mutual annihilation.

In a previous paper,[1] the AR was taken to increase with temperature, but this procedure was probably unjustified.[5] For temperatures so low that interstitial migration is rare, the effective AR would indeed increase with temperature, but as interstitials become freely migrating the vacancy sinks will lose their effectiveness and the effective AR will decrease.

---

* The principal difference between DEFECT, developed by Beeler, and Johnson's program is that a rigid boundary in the former replaces the elastic continuum of the latter.

Table 1. Vacancy Correlations, Nominal 800°K

| Defect | Jump Type | Activation Energy (ev) | Jump Probability Relative to Isolated $V_2$ |
|---|---|---|---|
| $V_1$ | Isolated jump | 1.32 | 0.002 |
| $V_1$[a] | One 2→1[b] | 1.28 | 0.004 |
| | Two 2→1 | 1.24 | 0.007 |
| | One 3→1 | 1.07 | 0.086 |
| | One 4→1 | 1.07 | 0.086 |
| | Two 3→1 | 0.82 | 1.0 |
| | Two 3→1 + One 4→1 | 0.57 | 1.0 |
| | Four 3→1 | 0.32 | 1.0 |
| $V_2$[c] | Isolated jump | 0.9 | 1.0 |
| $V_3$[c] | Reorientation | 0.9 | 1.0 |
| | Isolated jump | 1.02 | 0.165 |
| $V_4$[c] | Isolated jump | 1.15 | 0.024 |

[a] Correlating vacancies may be single or members of clusters.

[b] m→n designates jump from $m^{th}$ neighbor separation to $n^{th}$ neighbor separation.

[c] Data refer to one member of the cluster.

The approach in the present work was to study the sensitivity of the results to the AR by using two regions (see Table 2). The small AR is the 32 site spontaneous (0° K) annihilation region determined by Johnson; the large AR is a 104 site region obtained by moving one interstitial jump beyond the 32 site region.

Table 2. Annihilation Regions

Let split interstitial be located at origin and oriented in direction b.

| Neighbor | Type | Exceptions | Number |
|---|---|---|---|
| | Small Region (32 sites) | | |
| 1 | 110 | $\Delta b = 0$ | 8 |
| 3 | 211 | $\Delta b = \pm 2$ | 16 |
| 4 | 220 | $\Delta b = 0$ | 8 |
| | Large Region (104 sites) | | |
| 1 | 110 | $\Delta b = 0$ | 8 |
| 2 | 200 | $\Delta b \neq 0$ | 4 |
| 3 | 211 | $\Delta b = \pm 2$ | 16 |
| 4 | 220 | none | 12 |
| 5 | 310 | $\Delta b = 0$ | 16 |
| 6 | 222 | none | 8 |
| 7 | 321 | $\Delta b = \pm 2$ | 32 |
| 9 | 330 | $\Delta b = 0$ | 8 |

# 4 RESULTS AND DISCUSSION

## 4.1 High Temperature Displacement Cascades

4.1.1 Time History. As indicated above, computer runs were continued until defect interactions became infrequent--generally 1000 to 2000 time steps in each stage. One cascade was carried to 4000 time steps; in this case, no interactions occurred after 2000 steps.

Little annihilation took place in the vacancy stage relative to that in the interstitial stage, but there was a general increase in the fraction of mobile interstitials (see Figure 3). This occurs when a migrating vacancy interacts with an immobile interstitial cluster so as to reduce the cluster (or a portion of it) to size 3 or less. (Of course, there is general attrition of larger clusters also.) Several runs in which this phenomenon was prominent were continued in the interstitial mode to discover the fate of the newly created mobile defects. It was found that there is a strong tendency for these newly created defects to recluster with one another.

Decreasing the AR from 104 to 32 sites simply increased the rate of annihilation by the same factor that the defect population was increased; i.e., the percentage decrease per time step in the number of defects was the same in both bases.

4.1.2 Residual Annihilation and Clustering. The mutual annihilation of interstitials and vacancies that occurred during the short-term annealing simulation is summarized in Table 3. The number of residual defects was approximately 2 pair/keV between 5 and 20 keV for the large AR and ~4 pair/keV for the small AR. The cluster size distributions are given in Tables 4 and 5. With the large AR, 20-30%* of the surviving interstitials and 40-60% of the surviving vacancies are clustered. Most of the other defects migrate away and lose their identification with the cascade. The corresponding numbers for the small AR are 35-50% of the surviving interstitials and 60-70% of the surviving vacancies.

The spatial distribution of defects is illustrated in Figures 4 to 6. In each post-anneal configuration, the mobile interstitials have been removed in order to account for the $10^6$-$10^8$ jumps that each would have made, if permitted, during the vacancy stage. The quasi-channeled cascade of Figure 5 (in which no immobile interstitial clusters survived) was

---

* The percentage varied with cascade energy. In each case, the first number corresponds to 5 keV, the second to 20 keV.

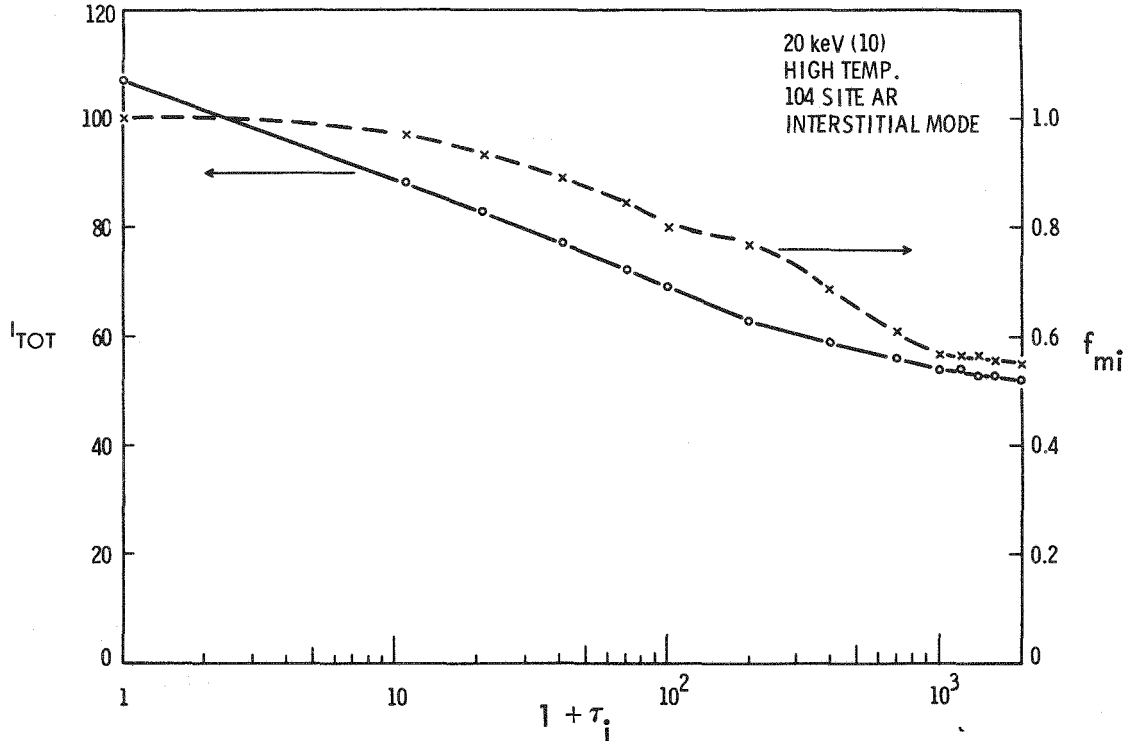


Figure 3-a.

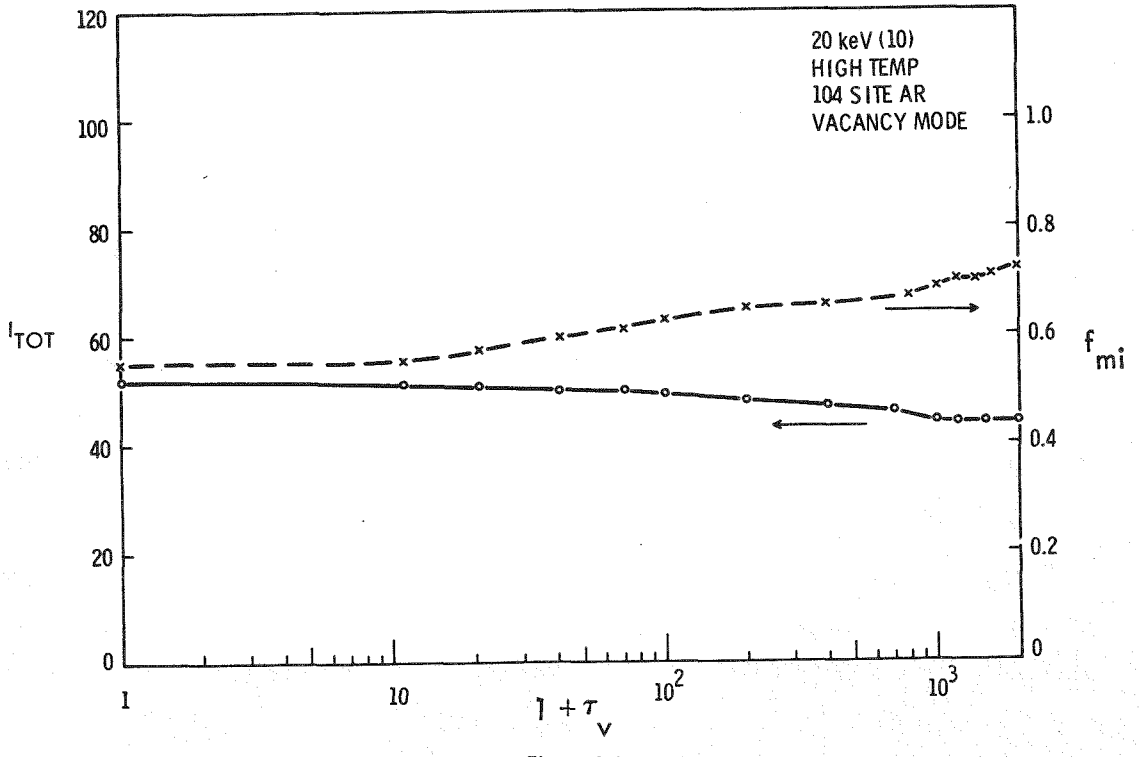


Figure 3-b.

Figure 3. The variation of the total number of interstitials ($I_{TOT}$) and the fraction of mobile interstitials ($f_{mi}$) with number of time steps, using the large annihilation region. (a) Interstitial migration stage. (b) Vacancy migration stage.

Table 3. Average Annihilation Characteristics

| Annealing Stage | Number of Defect Pairs | | | | | |
|---|---|---|---|---|---|---|
| | γ-Iron (Present Work) | | | | α-Iron (Ref. 1) | |
| | 20 keV | | 5 keV | | 20 keV | 5 keV |
| | Large AR[a] | Small AR[b] | Large AR[a] | Small AR[b] | (c) | (c) |
| CASCADE output | 406 | 406 | 93 | 93 | | |
| CASCADE output, 1st and 2nd neighbors annihilated | 253 | 253 | --- | --- | | |
| **High Temperature** | | | | | | |
| After initial annihilation | 107 | 188 | 25 | 50 | 140 | 40 |
| After interstitial stage | 52[d] | 102[d] | 12[d] | 22[e] | 50 | 13 |
| After vacancy stage | 43[f] | 79[f] | 11[f] | 19[g] | 42 | 12 |
| **Low Temperature** | | | | | | |
| After initial annihilation | 111 | 190 | - | 52 | 198 | 57 |
| After interstitial stage | 74[d] | 141[e] | - | 35[e] | 97 | 25 |

[a] 104 site AR.

[b] 32 site AR.

[c] 62 site AR for high temperature case; 30 site for low temperature case.

[d] 2000 steps in interstitial stage.

[e] 1000 steps in interstitial stage.

[f] Additional 2000 steps in vacancy stage.

[g] Additional 1000 steps in vacancy stage.

Table 4. Interstitial Cluster Size Distributions, High Temperature Case

| n | Number of Interstitial Clusters of Size n per Cascade | | | | | |
|---|---|---|---|---|---|---|
| | γ-Iron | | | | | |
| | 20 keV | | 5 keV | | α-Iron (Ref. 1) | |
| | Large AR[a] | Small AR[b] | Large AR[a] | Small AR[c] | 20 keV | 5 keV |
| 1 | 11.7 | 12.5 | 6.0 | 5.9 | | |
| 2 | 5.9 | 5.0 | 1.0 | 1.5 | | |
| 3 | 2.6 | 6.25 | 0.3 | 1.2 | | |
| 4 | 1.7 | 3.0 | 0.3 | 1.2 | | |
| 5 | 0.3 | 2.5 | 0.2 | 0.1 | | |
| 6 | 0.4 | 1.5 | 0 | 0 | | |
| 7 | 0.1 | 1.0 | 0 | 0.1 | | |
| 8 | 0.1 | 0 | 0 | 0.1 | | |
| 9 | 0 | 0 | 0 | 0 | | |
| 10 | 0 | 0.25 | 0 | 0 | | |
| ≥3 | 5.2 | 14.5 | 0.8 | 2.7 | 6.6 | 1.9 |
| ≥4 | 2.6 | 8.25 | 0.5 | 1.5 | 2.5 | 0.4 |
| ≥5 | 0.9 | 5.25 | 0.2 | 0.3 | 0.8 | 0 |
| n | Number of Interstitials in Clusters of Size ≥ n per Cluster | | | | | |
| 1 | 43.5 | 84.2 | 11.1 | 19.3 | 42.0 | 12.0 |
| 2 | 31.8 | 71.8 | 5.1 | 13.4 | 30.0 | 7.0 |
| 3 | 20.0 | 61.8 | 3.1 | 10.4 | 23.0 | 5.8 |
| 4 | 12.2 | 43.0 | 2.2 | 6.8 | 11.0 | 1.4 |
| 5 | 5.4 | 31.0 | 1.0 | 2.0 | 4.2 | 0 |
| 6 | 3.9 | 18.5 | 0 | 1.5 | 1.4 | 0 |

[a]Average of 10 cascades; 2000 interstitial + 2000 vacancy time steps.
[b]Average of 4 cascades; 1000 interstitial + 1000 vacancy time steps.
[c]Average of 10 cascades; 1000 interstitial + 1000 vacancy time steps.

Table 5. Vacancy Cluster Size Distributions, High Temperature Case

| n | Number of Vacancy Clusters of Size n per Cascade | | | | | |
|---|---|---|---|---|---|---|
| | γ-Iron | | | | | |
| | 20 keV | | 5 keV | | α-Iron (Ref. 1) | |
| | Large AR[a] | Small AR[b] | Large AR[a] | Small AR[a] | 20 keV | 5 keV |
| 1 | 10.2 | 15.2 | 3.8 | 4.8 | | |
| 2 | 1.2 | 1.75 | 0.6 | 0.8 | | |
| 3 | 0.6 | 0.25 | 0.3 | 0.4 | | |
| 4 | 0.6 | 1.0 | 0.1 | 0.1 | | |
| 5 | 1.3 | 1.5 | 0.2 | 0.3 | | |
| 6 | 0.6 | 1.75 | 0 | 0.1 | | |
| 7 | 0.9 | 0.5 | 0 | 0.2 | | |
| 8 | 0.3 | 1.0 | 0.1 | 0.1 | | |
| 9 | 0.4 | 0.5 | 0.1 | 0.1 | | |
| 10 | 0.2 | 0.25 | 0.1 | 0 | | |
| >10 | 0.2[c] | 1.75[d] | 0.1[e] | 0.5[f] | | |
| ≥4 | 4.5 | 8.25 | 0.7 | 1.4 | 3.7 | 1.0 |
| ≥7 | 2.0 | 4.0 | 0.4 | 0.9 | 1.8 | 0.5 |
| ≥10 | 0.4 | 2.0 | 0.2 | 0.6 | 0.7 | 0.12 |
| n | Number of Vacancies in Clusters of Size ≥ n per Cascade | | | | | |
| 1 | 43.4 | 84.2 | 11.1 | 19.2 | 42.0 | 12.0 |
| 4 | 29.0 | 64.5 | 5.2 | 11.6 | 26.4 | 6.7 |
| 7 | 16.5 | 42.5 | 3.8 | 9.1 | 17.2 | 4.0 |
| 10 | 4.2 | 26.5 | 2.1 | 6.0 | 8.4 | 1.2 |

[a] Average of 10 cascades.

[b] Average of 4 cascades.

[c] $2V_{11}$ in 10 cascades.

[d] $V_{11}$, $3V_{12}$, $V_{13}$, $V_{14}$, $V_{22}$ in 4 cascades.

[e] $V_{11}$ in 10 cascades.

[f] $5V_{12}$ in 10 cascades.

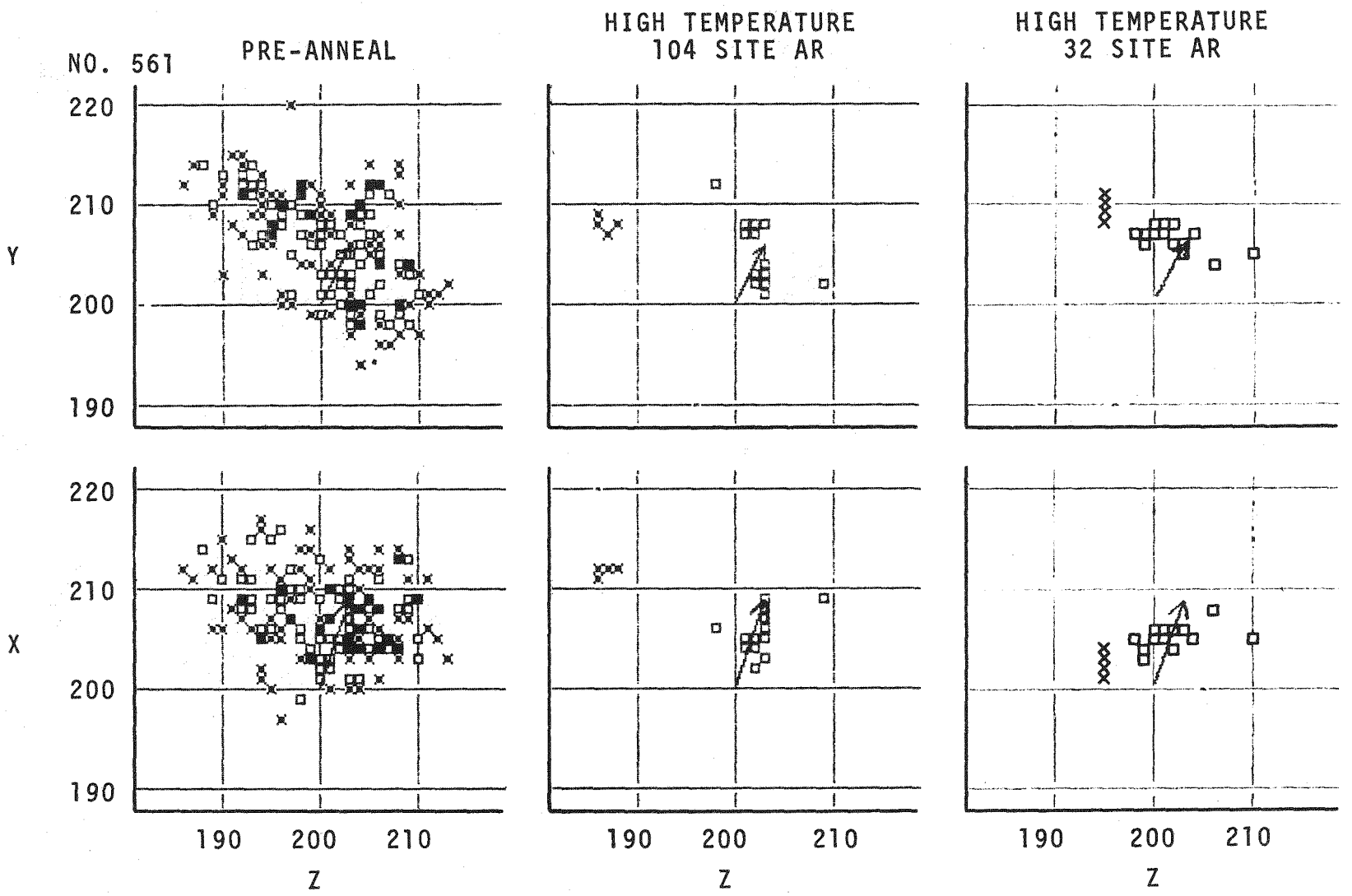


Figure 4. A projection onto two planes of pre-anneal and high temperature post-anneal configurations of a 5 keV cascade for two annihilation regions. Squares and Xs are vacancies and interstitials, respectively. Take-off point of PKA is 200, 200, 200; direction is shown by arrow. Dimension is half-lattice constant.

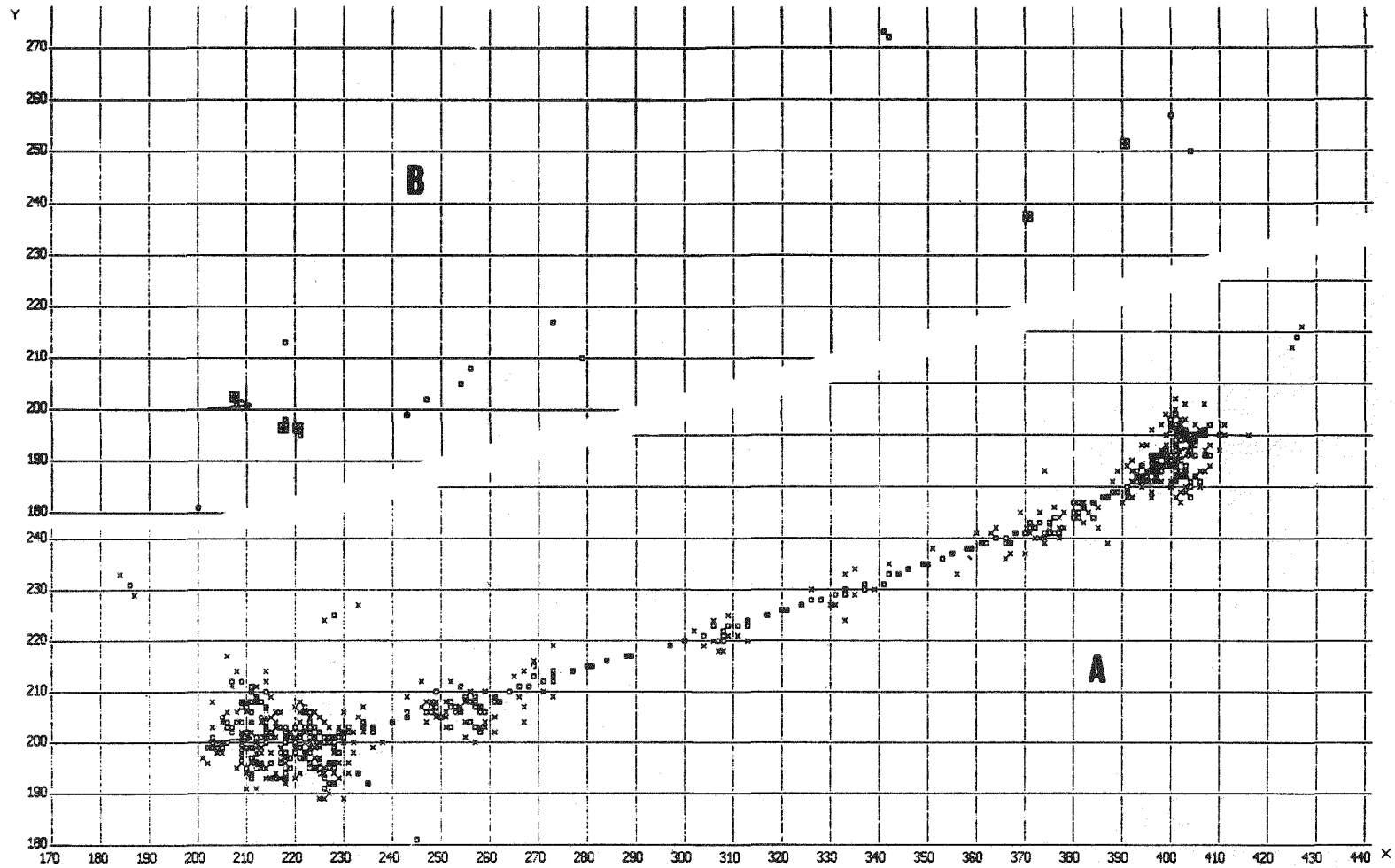


Figure 5. A quasi-channeled 20 keV cascade (No. 2079). See caption Figure 4. (a) Pre-anneal. (b) High temperature post-anneal, 104 site AR.

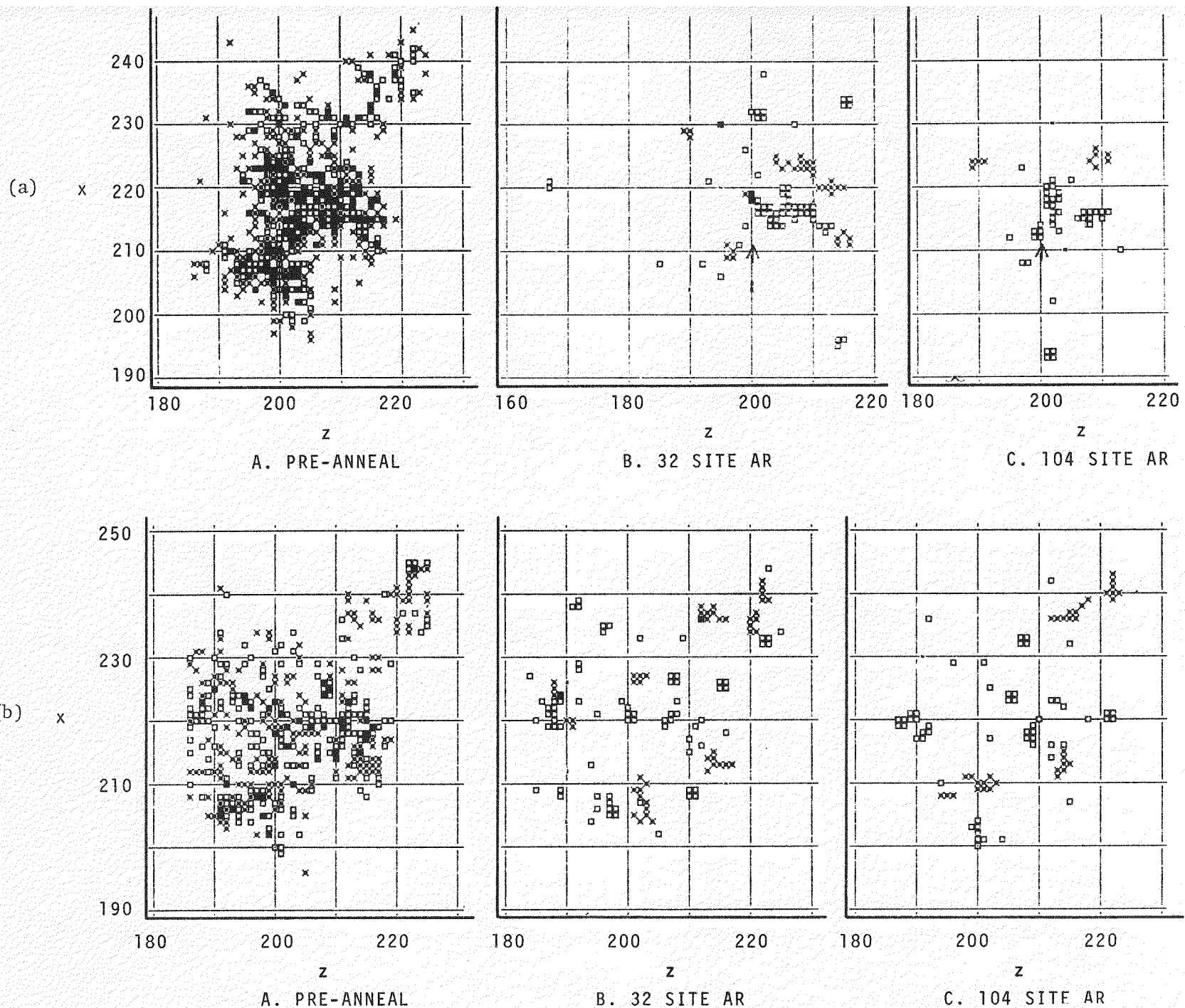


Figure 6. (a) A compact 20 keV cascade (No. 2076). (b) A "randomized cascade" (No. 77) in the geometry of cascade No. 2076. High temperature anneals. See caption Figure 4.

the only one of its type studied. More common was the rather compact cascade shown in Figure 6a which served as the model for the randomized cascade. In regard to 5 keV cascades, it was not uncommon to have no residual immobile interstitial clusters (i.e., $I \geq 4$) or vacancy clusters ($V \geq 5$) when the large AR was used.

4.1.3 Effect of Annihilation Region. Results for large and small ARs are directly compared for 20 keV cascades in Figure 7. Plotted are the fractional distributions of residual defects (i.e., each sums to unity) in clusters to show the influence of the AR on the relative clustering within a cascade. An absolute comparison is easily made using Tables 3 to 5. The small AR promoted clustering of both interstitials and vacancies (the largest vacancy cluster was a $V_{22}$). The results for 5 keV cascades were similar, but shifted somewhat toward smaller cluster sizes.

4.1.4 Energy Dependence. Fractional defect distributions for 20 and 5 keV cascades are compared in Tables 4 and 5. At 5 keV, there are relatively more single interstitials and fewer large clusters. Maximum interstitial cluster sizes were 8 and 5 for 20 and 5 keV, respectively, for the large AR and 10 and 8, respectively, for the small AR. The number of interstitial clusters generally increased faster than the energy for the two energy values investigated; e.g., the number of clusters of size $\geq 4$ was proportional to $E^{1.2}$.

In the case of vacancies, 5 keV cascades had proportionately more small clusters than 20 keV cascades and also proportionately more large clusters. The latter was especially true for the large AR, for which the maximum cluster size was 11 at each energy. The small AR resulted in maximum cluster sizes of 22 and 12 for 20 and 5 keV cascades, respectively.

The number of vacancy clusters generally increased faster than the energy, as for interstitials. For clusters of size $\geq 4$ (or $\geq 5$) the number per cascade was proportional to $E^{1.3}$.

4.2 Randomized Cascades

4.2.1 Time History. Two randomized cascades, patterned after the same displacement cascade but with independent defect configurations, were run in high temperature simulations with both large and small AR. The rate of annihilation was the same as for the corresponding displacement cascade runs. The decrease in the fraction of mobile interstitials with time during the interstitial stage, however, was surprisingly sensitive to the value of the AR, and the rate of decrease was higher than the average rate exhibited by the real displacement cascades for either value of the AR.

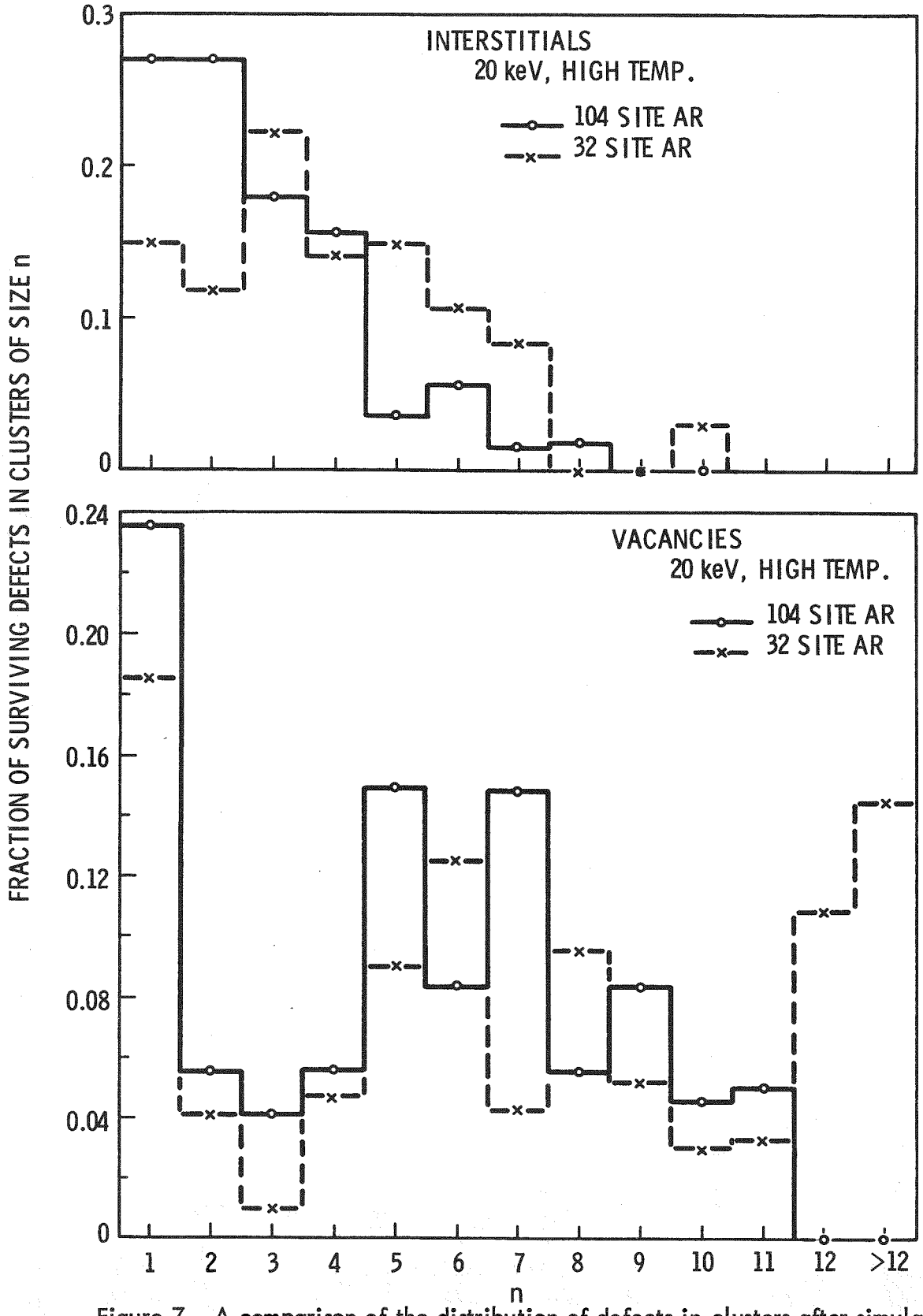


Figure 7. A comparison of the distribution of defects in clusters after simulated high temperature anneals using small and large annihilation regions. The small AR vacancy distribution extends to clusters of size 22.

4.2.2 Residual Annihilation and Clustering. The results of mutual annihilation for the randomized cascades is summarized in Table 6. The small AR resulted in 70% more residual defects than the large AR.

Clustering of defects in randomized cascades is summarized in Table 7. The creation of mobile interstitials in the vacancy stage was common in these runs, particularly for the small AR case; hence the distributions overemphasize somewhat the small cluster sizes.

Cluster size distributions for randomized cascades and actual cascades are compared in Figure 8 and 9. There is a significant difference in sensitivity to the AR in the two cases. The randomized cascades were sensitive only at the large cluster end of the distributions for both interstitials and vacancies. The maximum interstitial cluster size was decreased somewhat while the maximum vacancy cluster size was increased by decreasing the AR. Actual cascades, on the other hand, exhibited a decrease in small clusters and an increase in large clusters when the AR was decreased. It is this difference in behavior that gives rise to the AR effect that is apparent in Figures 8 and 9.

The decreased influence of a change in the AR on the randomized cascades is probably a result of the more uniform spatial distribution of defects in this case. It appears that the mean distance between interstitials is significantly increased and hence clustering decreased by increasing the AR in the case of actual cascades, but not for randomized cascades. The same is true for vacancies, but the bunching of vacancies in actual cascades (as, for example, in Figure 1) causes enhanced vacancy clustering for either AR relative to the randomized cascades.

The spatial distribution of defects in one of the randomized cascades is shown in Figure 6b for direct comparison with Figure 6a. The difference in interstitial clustering is particularly evident.

## 4.3 Low Temperature Displacement Cascades

4.3.1 Time History. The evolution with time of the low temperature configurations (see Figures 10 and 11) is qualitatively predictable from the high temperature behavior. The annihilation rate was lower because of the absence of migrating di- and tri-interstitials. On the other hand, the mobile fraction of interstitials decreased more rapidly for the same reason. The effect of changing the AR was the same as for the high temperature runs.

Table 6. Average Annihilation Characteristics of Randomized Cascades, High Temperature

| Annealing Stage | Number of Defect Pairs | |
|---|---|---|
| | Large AR | Small AR |
| Initial loading--1st and 2nd neighbor annihilation | 257 | 257 |
| After complete initial annihilation | 118 | 186 |
| After interstitial stage (1000 steps) | 62 | 111 |
| After vacancy stage (1000 steps) | 54 | 91 |

Table 7. Cluster Size Distributions for Randomized Cascades, High Temperature

| Number of Clusters of Size n per Randomized Cascade[a] | | | | | |
|---|---|---|---|---|---|
| Interstitials | | | Vacancies | | |
| n | Large AR | Small AR | n | Large AR | Small AR |
| 1 | 5.0 | 9.5 | 1 | 19.0 | 35.5 |
| 2 | 4.0 | 5.0 | 2 | 1.0 | 3.5 |
| 3 | 2.0 | 7.5 | 3 | 0 | 1.5 |
| 4 | 3.0 | 2.0 | 4 | 3.0 | 2.5 |
| 5 | 1.5 | 1.5 | 5 | 2.0 | 1.0 |
| 6 | 1.0 | 3.5 | 6 | 0 | 1.0 |
| 7 | 0 | 1.0 | 7 | 1.0 | 1.5 |
| 8 | 0.5 | 0 | 8 | 0.5 | 0 |
| 9 | 0 | 0 | 9 | | 0 |
| 10 | 0 | 0.5 | 10 | | 0 |
| >10[b] | 0.5 | | >10 | | 1.0[c] |
| ≥3 | 8.5 | 16.0 | ≥4 | 6.5 | 7.0 |
| ≥4 | 6.5 | 8.5 | ≥7 | 1.5 | 2.5 |
| ≥5 | 3.5 | 6.5 | ≥10 | 0 | 1.0 |
| Number of Defects in Clusters of Size ≥ n per Randomized Cascade | | | | | |
| 1 | 54.0 | 90.5 | 1 | 54.0 | 90.5 |
| 2 | 49.0 | 81.0 | 4 | 33.0 | 43.5 |
| 3 | 41.0 | 71.0 | 7 | 11.0 | 22.5 |
| 4 | 35.0 | 48.5 | 10 | 0 | 12.0 |
| 5 | 23.0 | 40.5 | | | |
| 6 | 15.5 | 33 | | | |

[a] Average of two "cascades"

[b] 1-$I_{11}$ in two "cascades"

[c] 1-$V_{11}$ and 1-$V_{13}$ in two "cascades"

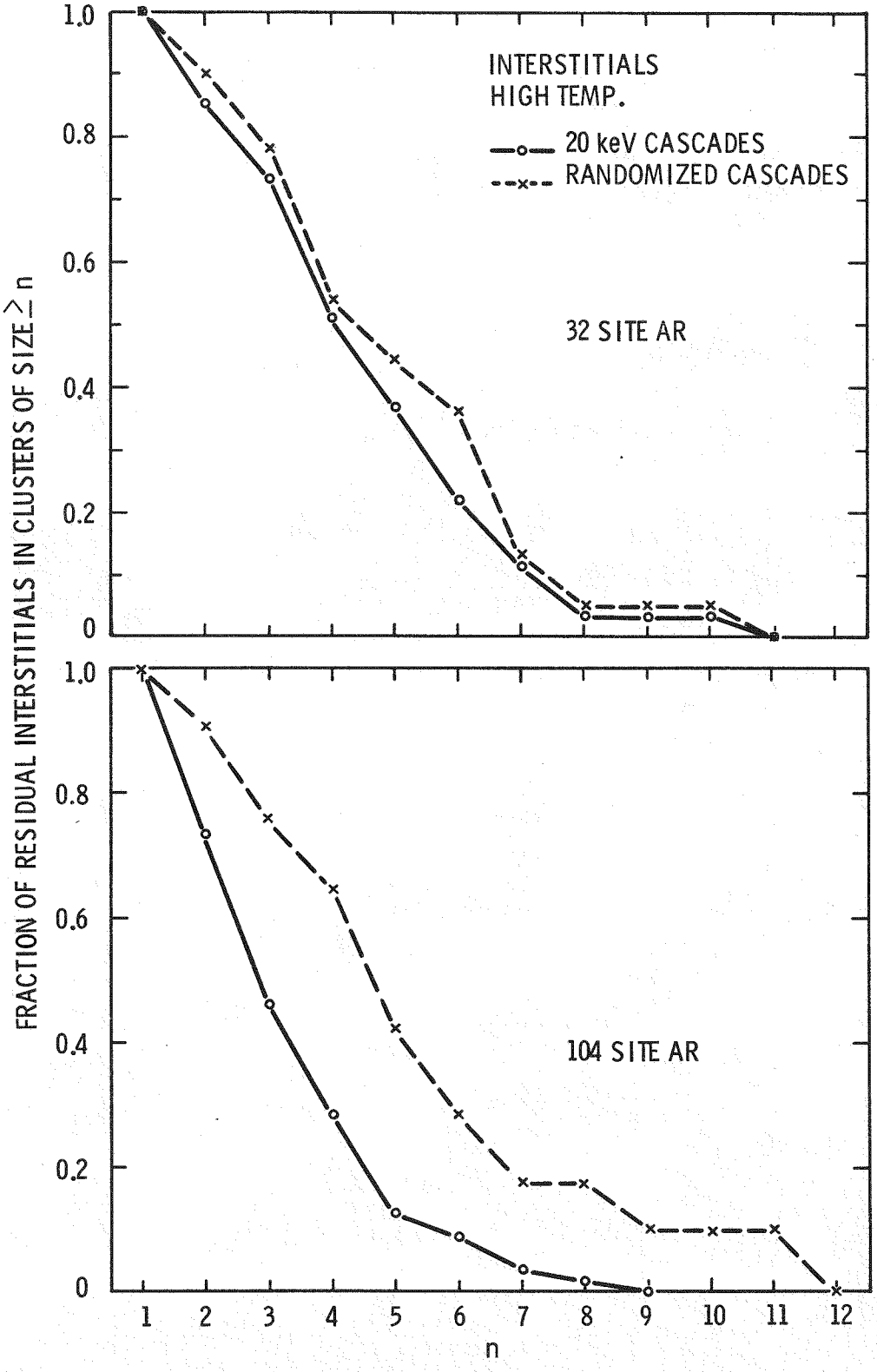


Figure 8. A comparison of integral distributions of interstitials in clusters for displacement cascades and "randomized cascades."

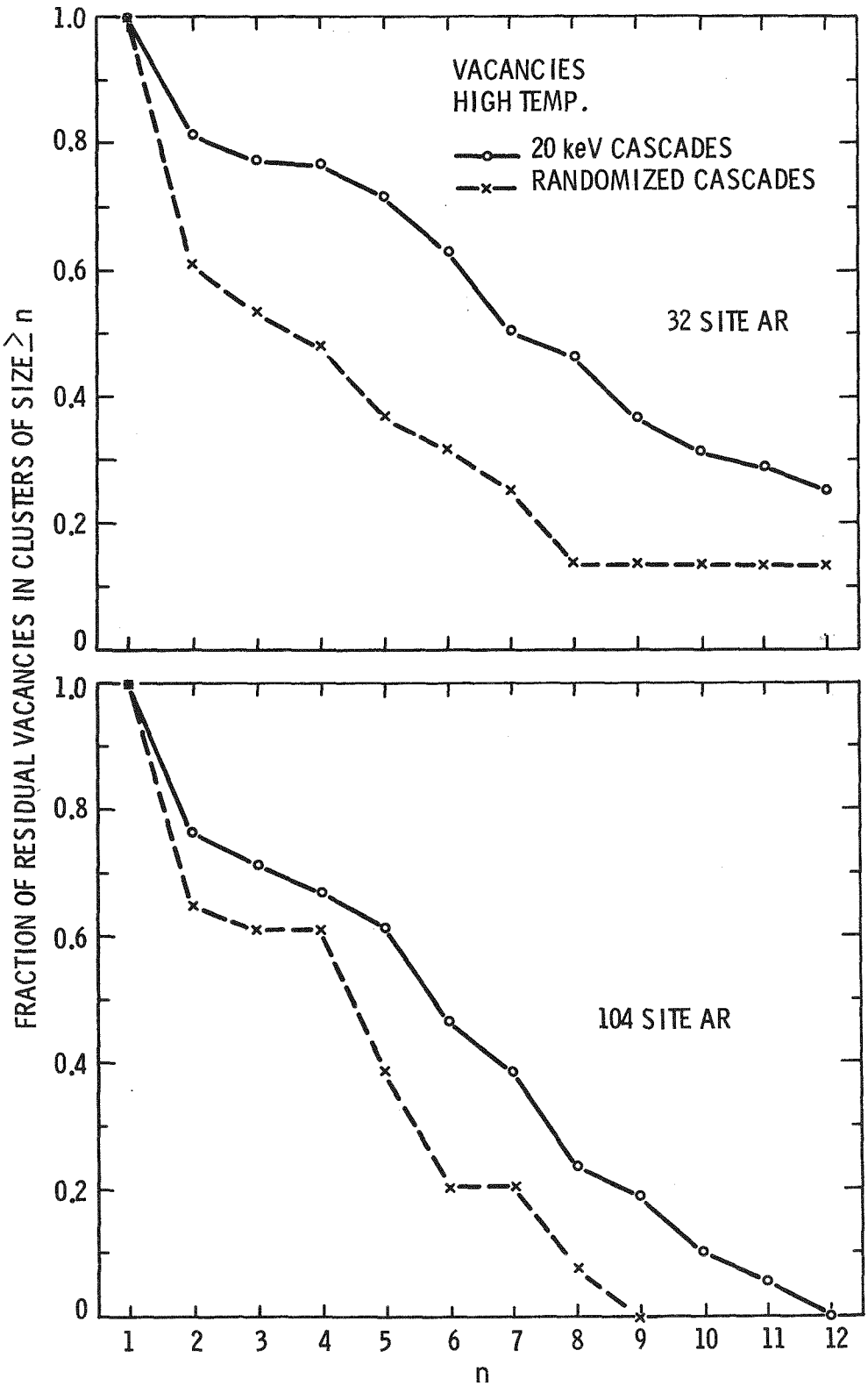


Figure 9. A comparison of integral distributions of vacancies in clusters for displacement cascades and "randomized cascades."

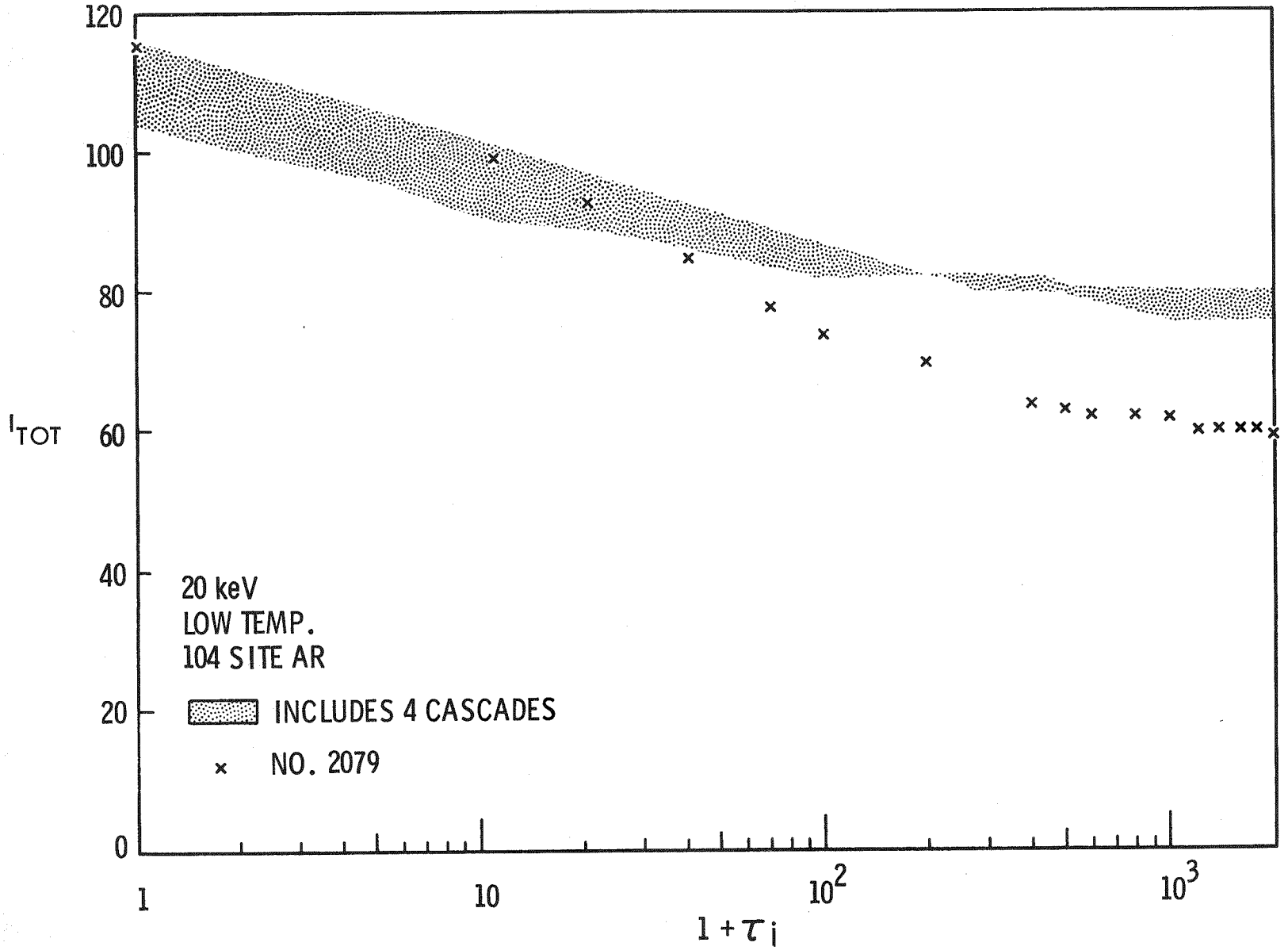


Figure 10. The variation of the total number of interstitials ($I_{TOT}$) with number of time steps, using the large annihilation region in a low temperature simulation. The quasi-channeled cascade (No. 2079) exhibits greater annihilation because clustering is inhibited (see Figure 11).

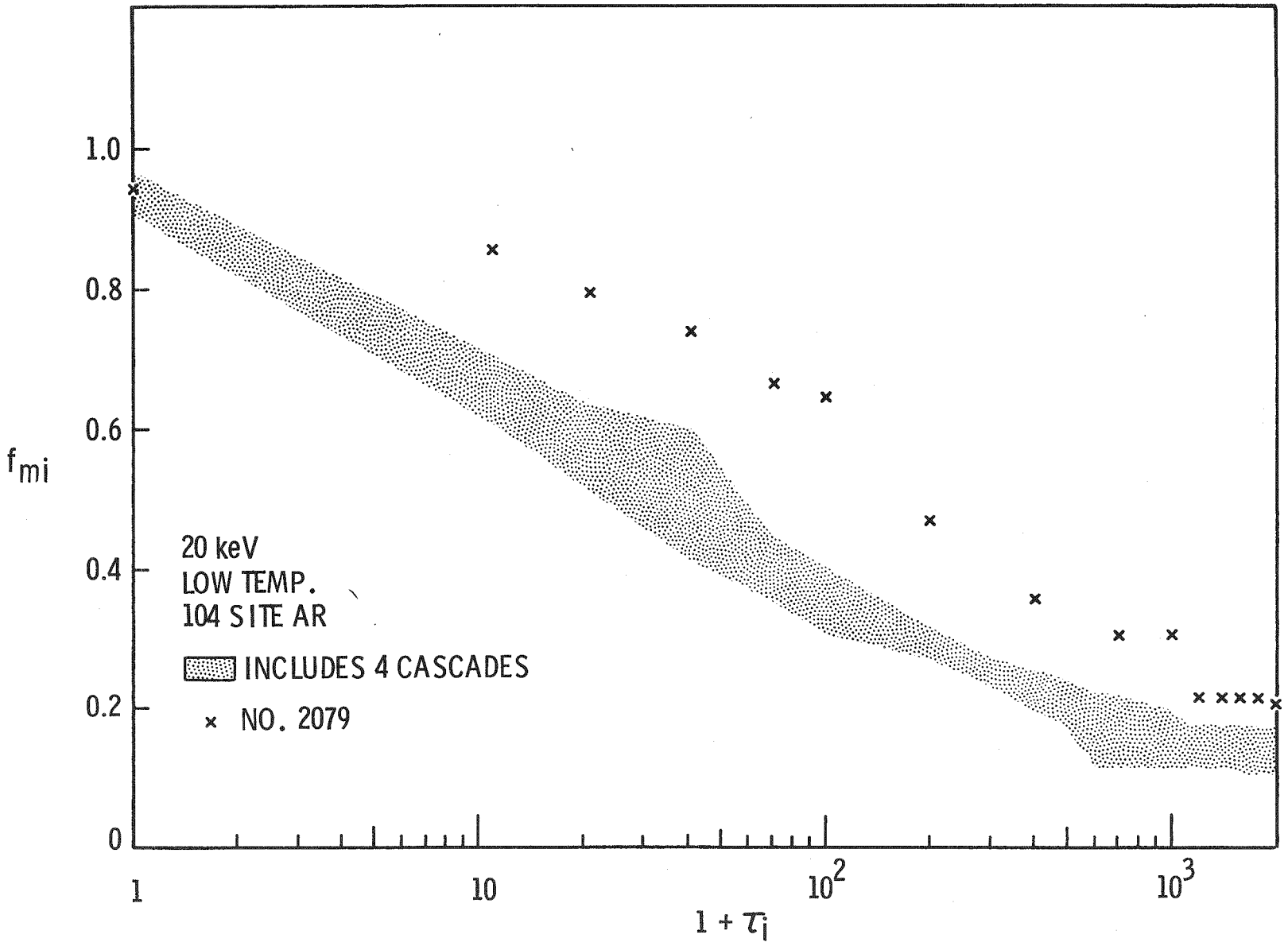


Figure 11. The variation of the fraction of mobile interstitials ($f_{mi}$) with number of time steps, using the large annihilation region in a low temperature simulation. Clustering in the quasi-channeled cascade (No. 2079) lags behind that in the more compact cascades.

4.3.2 Residual Annihilation and Clustering. The decreased effect of mutual annihilation in the low temperature case is evident in Table 3. The number of defect pairs surviving the annealing was 3.7/keV and 7/keV for the large and small AR, respectively. Only 10-14% of the interstitials remain unclustered (i.e., single) in the low temperature case and the maximum cluster size is 6 for large and small AR (see Table 8 and Figure 12). Decreasing the AR promotes clustering of interstitials.

Vacancy clusters experience only attrition, of course, in a low temperature anneal. The tendency toward shifting the cluster size distribution toward smaller sizes is mild for the small AR but pronounced for the large AR (see Table 9 and Figure 12). At 20 keV, the number of vacancy clusters of size 4 or greater dropped from a pre-anneal value of 12.4 to 7 and 3.4 for the small and large ARs, respectively.

The spatial distribution of defects after a low temperature anneal is illustrated in Figures 13 through 15.

4.3.3 Energy Dependence. The energy dependence was not studied thoroughly in the low temperature case. Only one 5 keV cascade was processed, for which the small AR was used (see Tables 8 and 9). The residual number of defects was just one-fourth of the number found for 20 keV cascades. The cluster size distributions are consistent with the energy dependence at high temperature (see Section 4.1.4).

4.4 Temperature Dependence

The differences between the cluster size distributions resulting from low and high temperature anneals can be seen in Figures 16 through 19 for both ARs. The pre-anneal distributions are included also.

To more clearly separate the effect of temperature on the relative distributions of defects in clusters vis-a-vis the absolute number of residual defects, integral distributions normalized to unity are presented in Figures 20 and 21.

The low temperature anneal resulted in 75% more residual defects than did the high temperature anneal. While Figures 20 and 21 show clearly that, for both ARs, clustering of both kinds of defects was favored at high temperature, the difference in the actual number of clustered defects present at low and high temperatures is less pronounced because of the fewer residual defects in the high temperature case.

TABLE 8. Interstitial Cluster Size Distributions, Low Temperature Case

| n | Number of Interstitial Clusters of Size n per Cascade | | | | |
|---|---|---|---|---|---|
| | γ-Iron | | | | |
| | 20 keV[a] | | 5 keV[b] | α-Iron (Ref. 1) | |
| | Large AR | Small AR | Small AR | 20 keV | 5 keV |
| 1 | 11.0 | 15.4 | 7 | | |
| 2 | 11.4 | 21.2 | 9 | | |
| 3 | 8.2 | 14.6 | 0 | | |
| 4 | 2.6 | 6.2 | 0 | | |
| 5 | 0.6 | 2.0 | 2 | | |
| 6 | 0.2 | 0.8 | | | |
| $\geq$3 | 12.0 | 23.6 | 2 | 19.8 | 4.6 |
| $\geq$4 | 3.4 | 9.0 | 2 | 10.7 | 1.8 |
| $\geq$5 | 0.8 | 2.8 | 2 | 4.0 | 0.8 |
| n | Number of Interstitials in Clusters of Size $\geq$n per Cascade | | | | |
| 1 | 74.2 | 141.0 | 35 | 98 | 25 |
| 2 | 63.2 | 126.0 | 28 | 80.6 | 18 |
| 3 | 40.4 | 83.4 | 10 | 79 | 17 |
| 4 | 14.6 | 39.6 | 10 | 50.8 | 8.6 |
| 5 | 4.2 | 14.8 | 10 | 22.8 | 4.6 |
| 6 | 1.2 | 4.8 | 0 | 11.2 | 3.3 |

[a]Average of 5 cascades; 2000 time steps for large (104 site) AR, 1000 for small (32 site) AR.

[b]A single cascade; 2000 time steps (no change after 400).

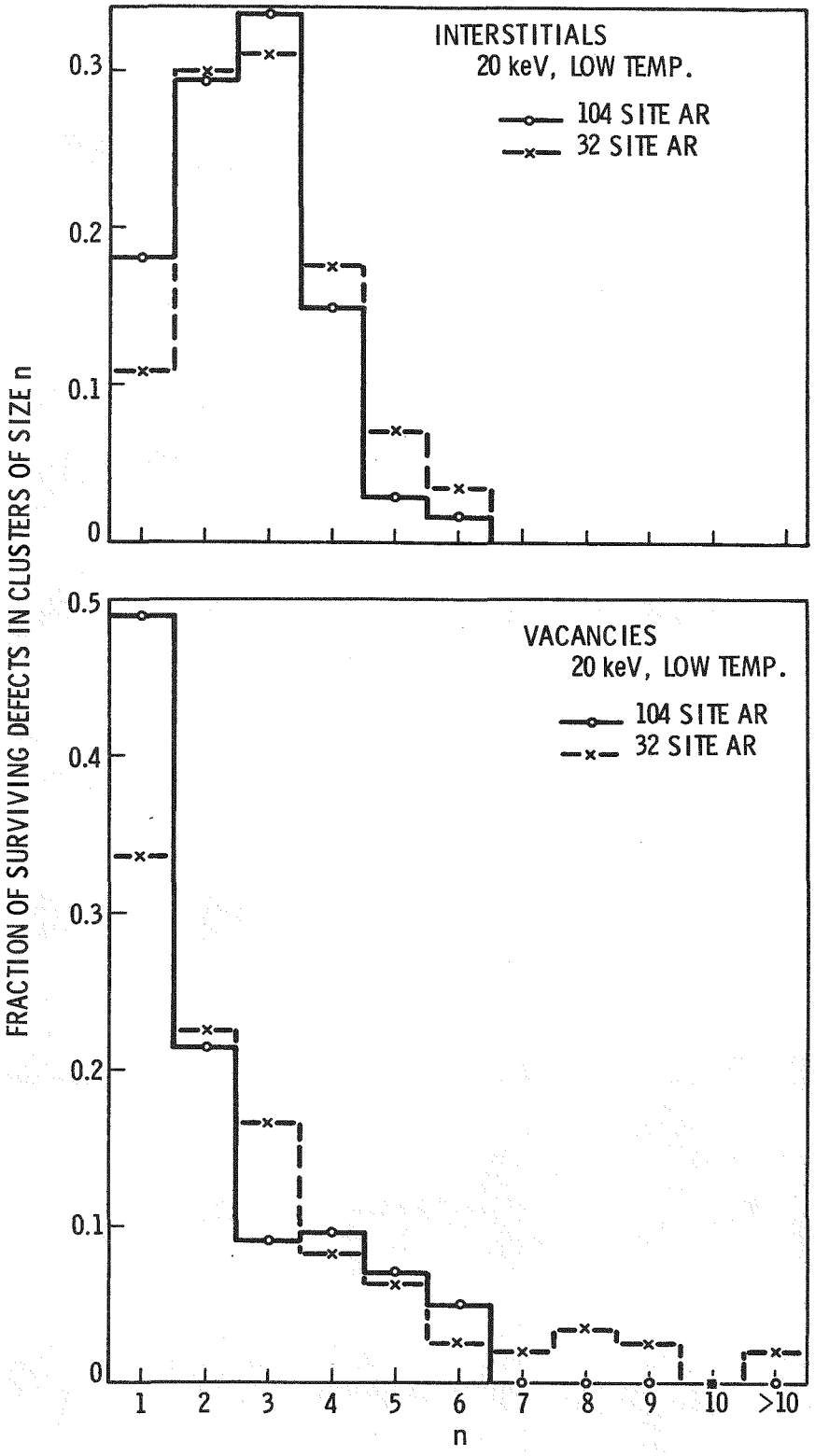


Figure 12. A comparison of the distribution of defects in clusters after simulated low temperature anneals using small and large annihilation regions.

TABLE 9. Vacancy Cluster Size Distributions, Low Temperature Case

| n | Number of Vacancy Clusters of Size n per Cascade | | | | |
|---|---|---|---|---|---|
| | γ-Iron | | | | |
| | 20 keV[a] | | 5 keV[b] | α-Iron (Ref. 1) | |
| | Large AR | Small AR | Small AR | 20 keV | 5 keV |
| 1 | 36.0 | 47.4 | 15 | | |
| 2 | 7.8 | 15.8 | 2 | | |
| 3 | 2.2 | 7.8 | 3 | | |
| 4 | 1.8 | 3.0 | 0 | | |
| 5 | 1.0 | 1.8 | 0 | | |
| 6 | 0.6 | 0.6 | 0 | | |
| 7 | 0 | 0.4 | 1 | | |
| 8 | 0 | 0.6 | 0 | | |
| 9 | 0 | 0.4 | 0 | | |
| 10 | 0 | 0 | 0 | | |
| >10 | 0 | 0.2[c] | 0 | | |
| ≥4 | 3.4 | 7.0 | 1 | 2.9 | 0.9 |
| ≥7 | 0 | 1.6 | 1 | 0.11 | 0 |
| ≥10 | 0 | 0.2 | 0 | 0.11 | 0 |
| n | Number of Vacancies in Clusters of Size ≥n per Cascade | | | | |
| 1 | 74.0 | 141.0 | 35 | 98.0 | 24.0 |
| 4 | 15.8 | 38.6 | 7 | 14.6 | 4.6 |
| 7 | 0 | 14.0 | 7 | 2 | 0 |
| 10 | 0 | 2.8 | 0 | 2 | 0 |

[a] Average of 5 cascades.

[b] A single cascade.

[c] $V_{14}$ in 5 cascades.

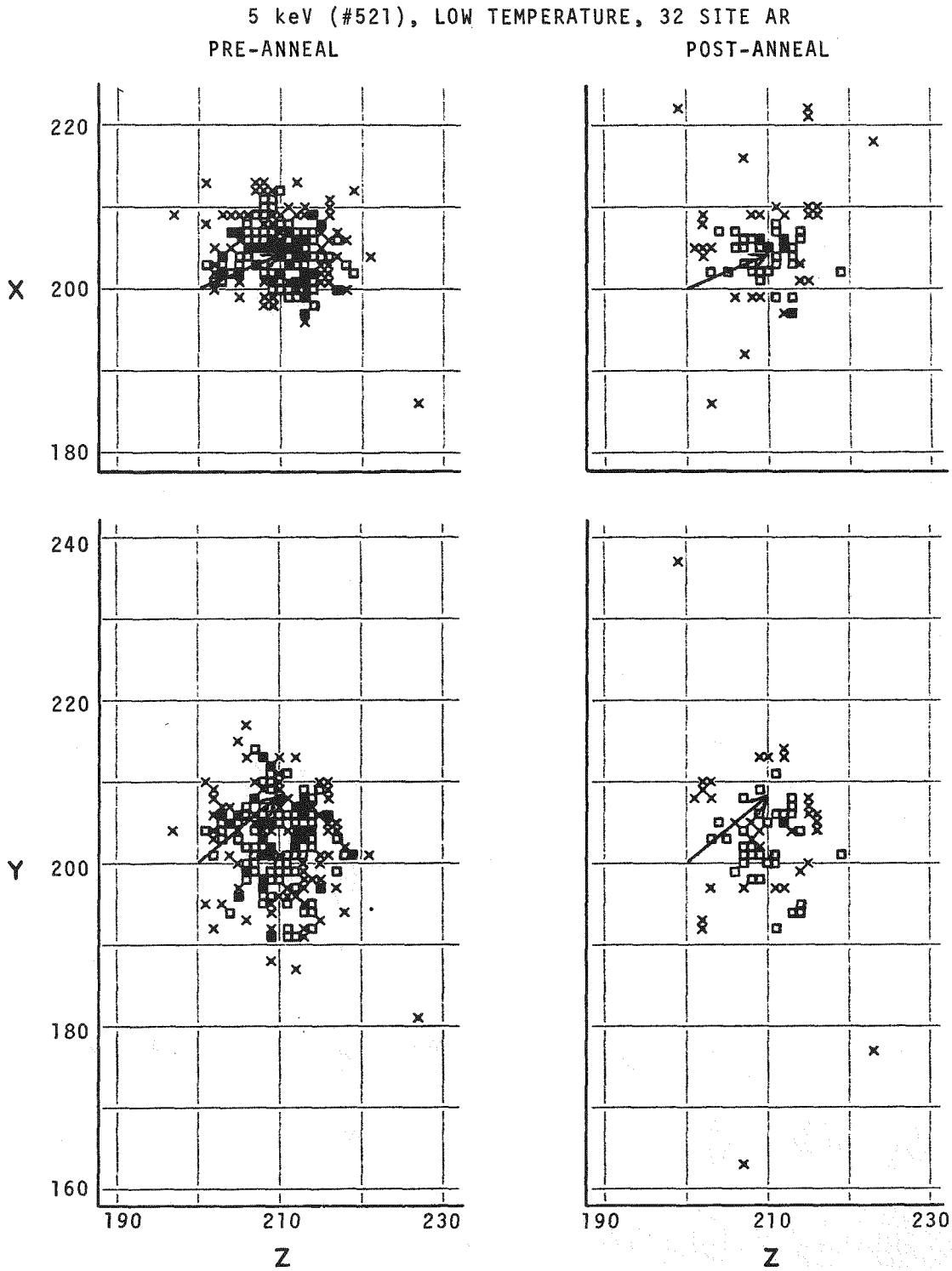


Figure 13. A projection onto two planes of pre-anneal and low temperature post-anneal configurations of a 5 key cascade (small annihilation region). See caption Figure 4.

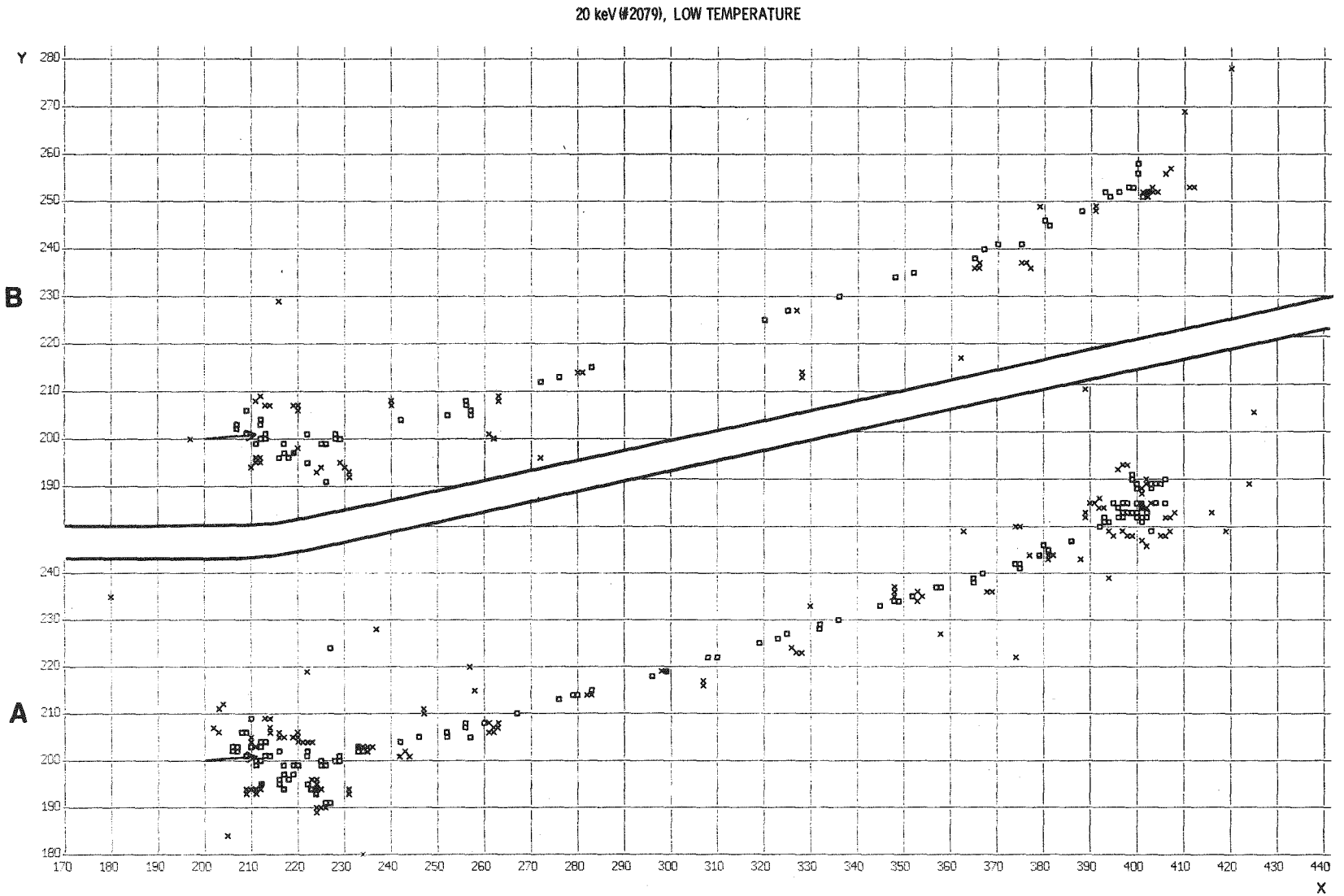


Figure 14. The quasi-channeled cascade (No. 2079) of Figure 5 after a low temperature anneal. (a) 32 site AR. (b) 104 site AR.

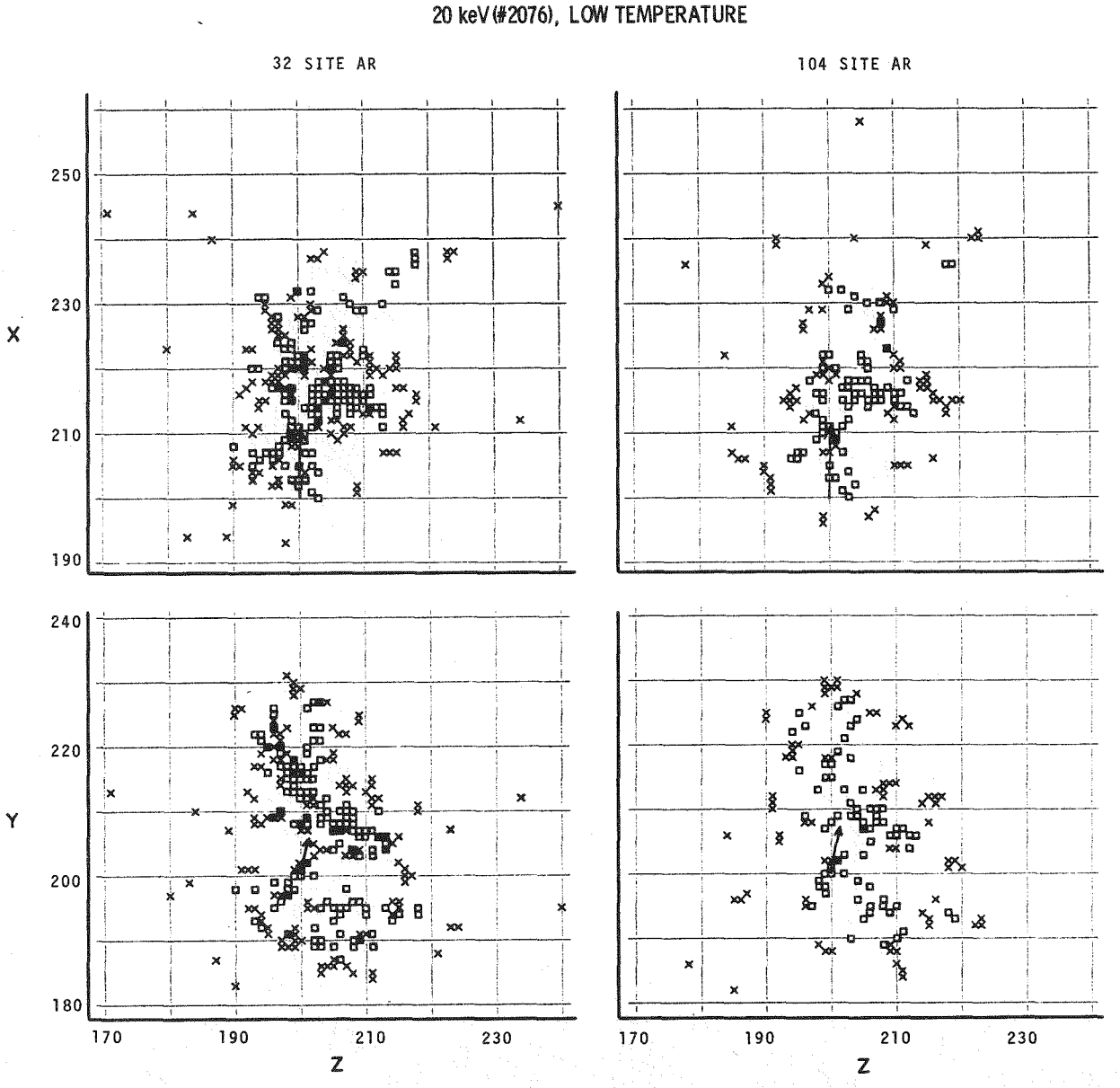


Figure 15. The compact cascade (No. 2076) of Figure 6-a after low temperature anneals with small and large annihilation regions.

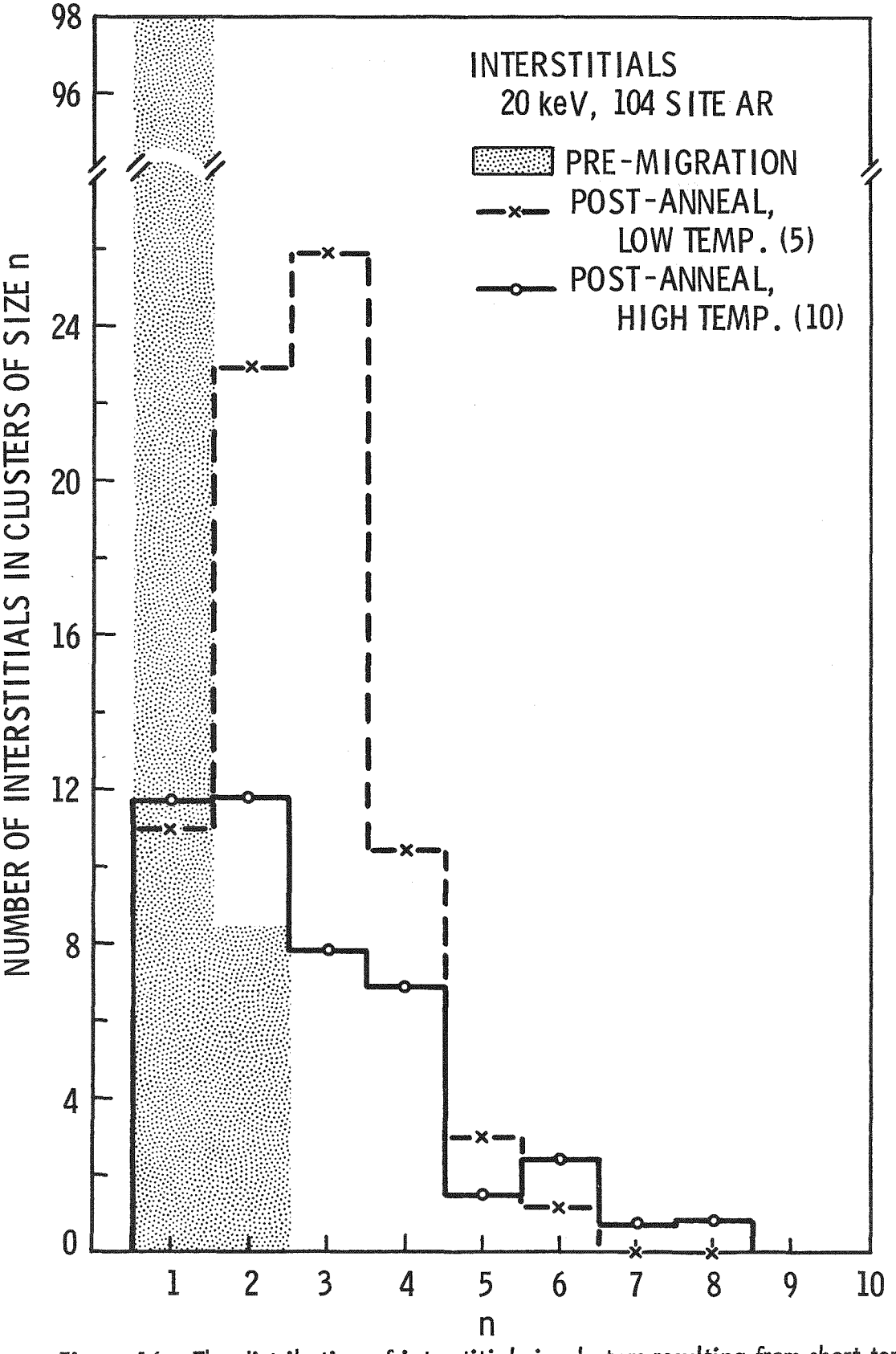


Figure 16. The distribution of interstitials in clusters resulting from short term anneals at low and high temperatures with a 104 site annihilation region.

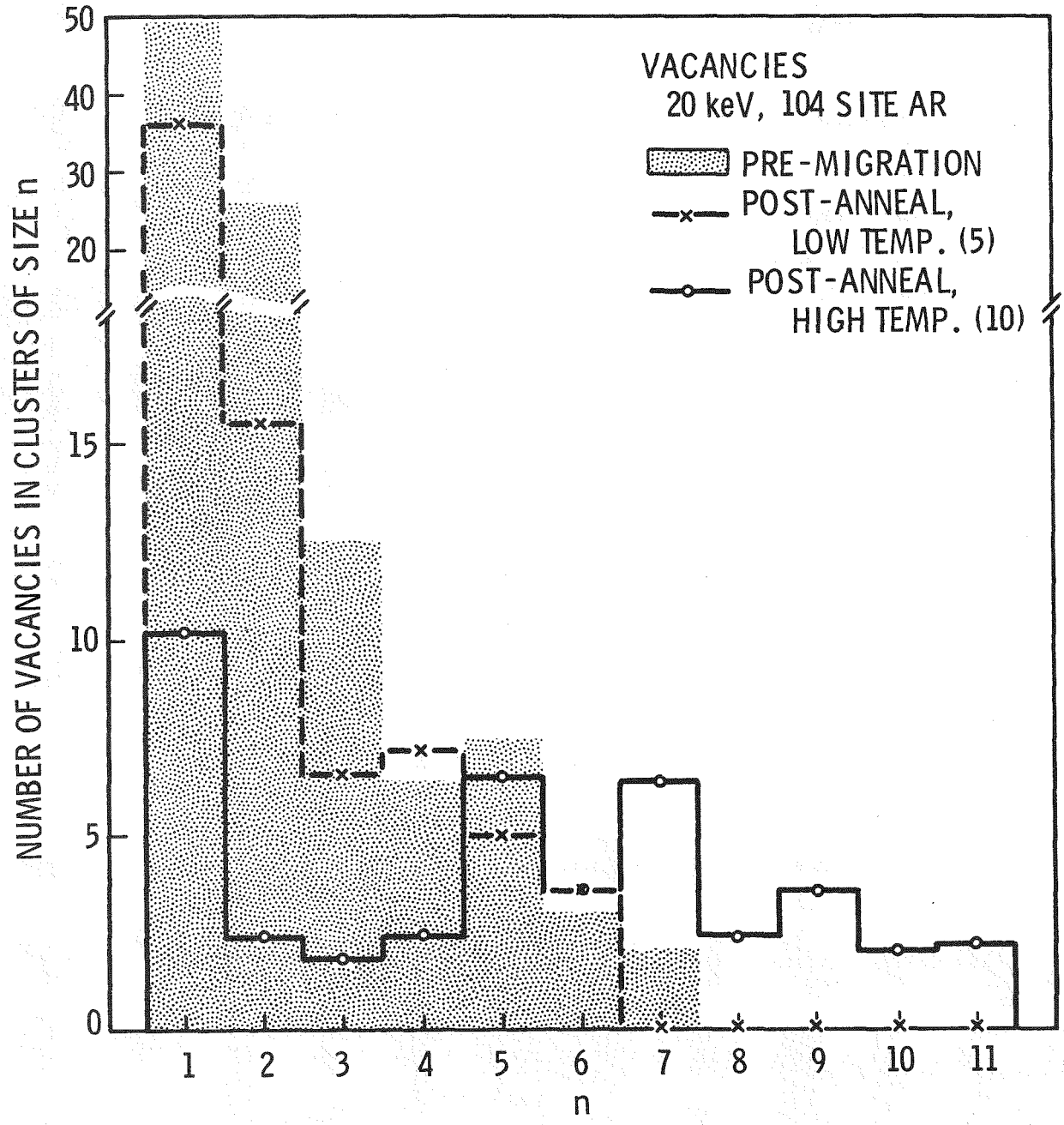


Figure 17. The distribution of vacancies in clusters resulting from short term anneals at low and high temperatures with a 104 site annihilation region.

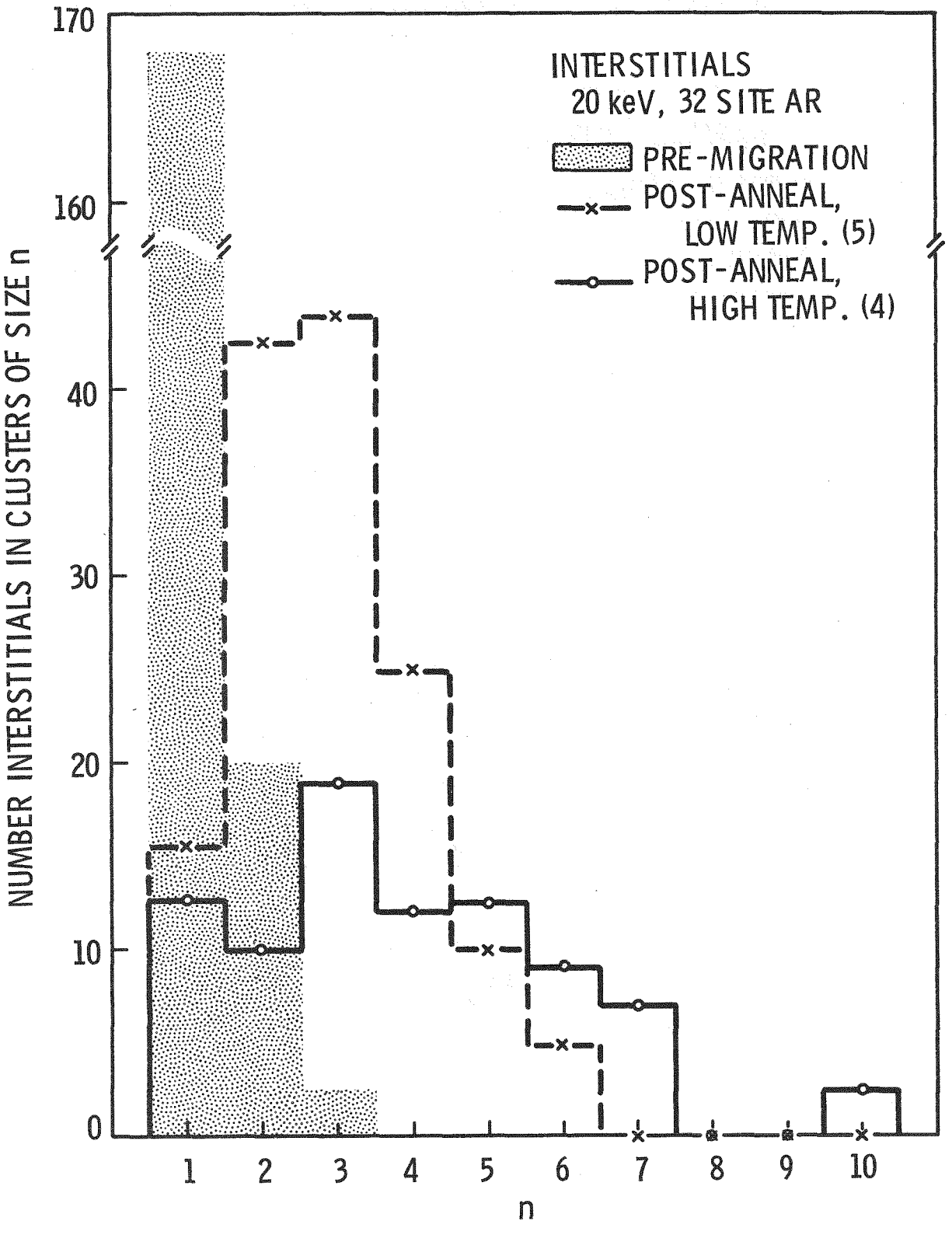


Figure 18. The distribution of interstitials in clusters resulting from short term anneals at low and high temperatures with a 32 site annihilation region.

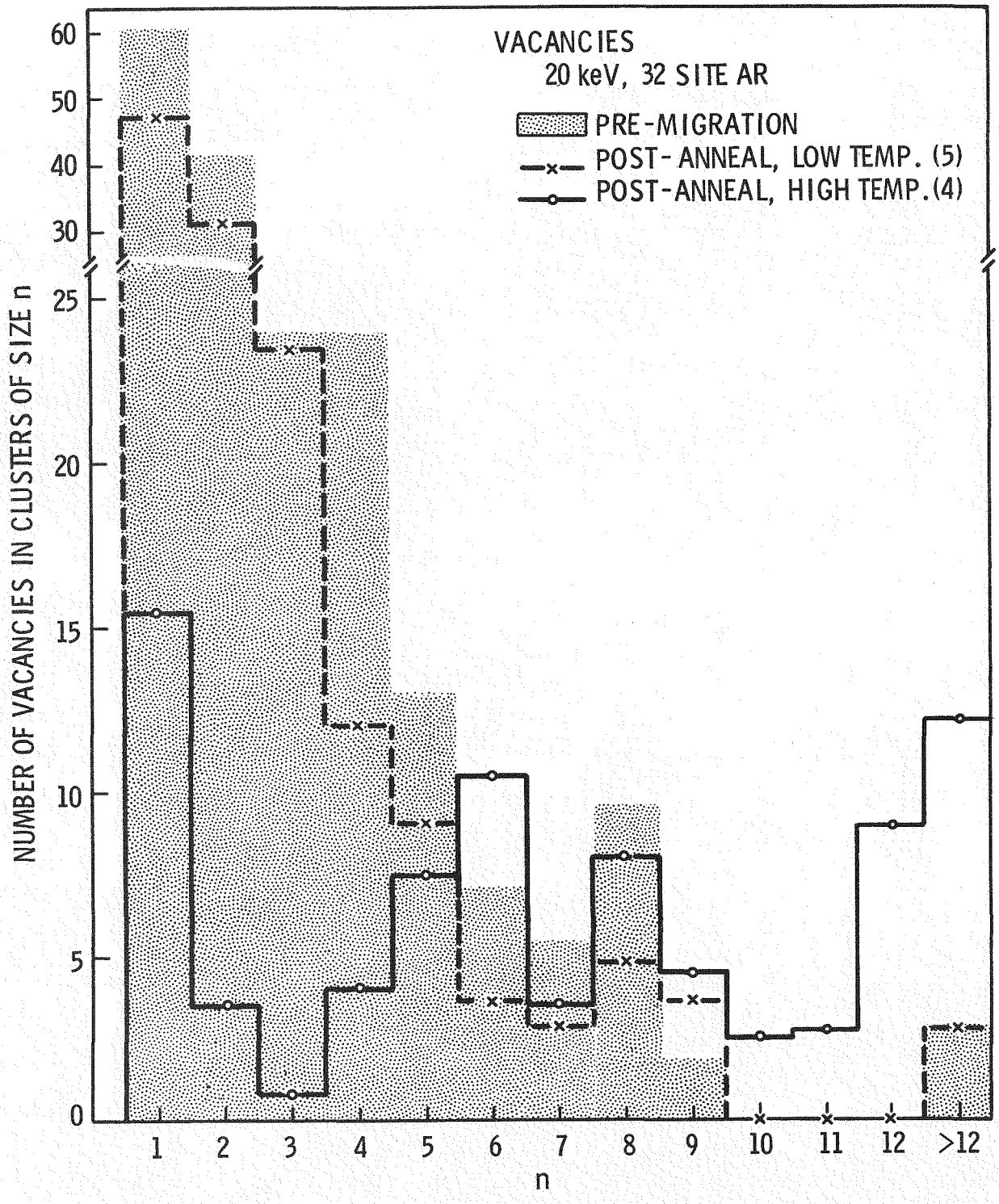


Figure 19. The distribution of vacancies in clusters resulting from short term anneals at low and high temperatures with a 32 site annihilation region.

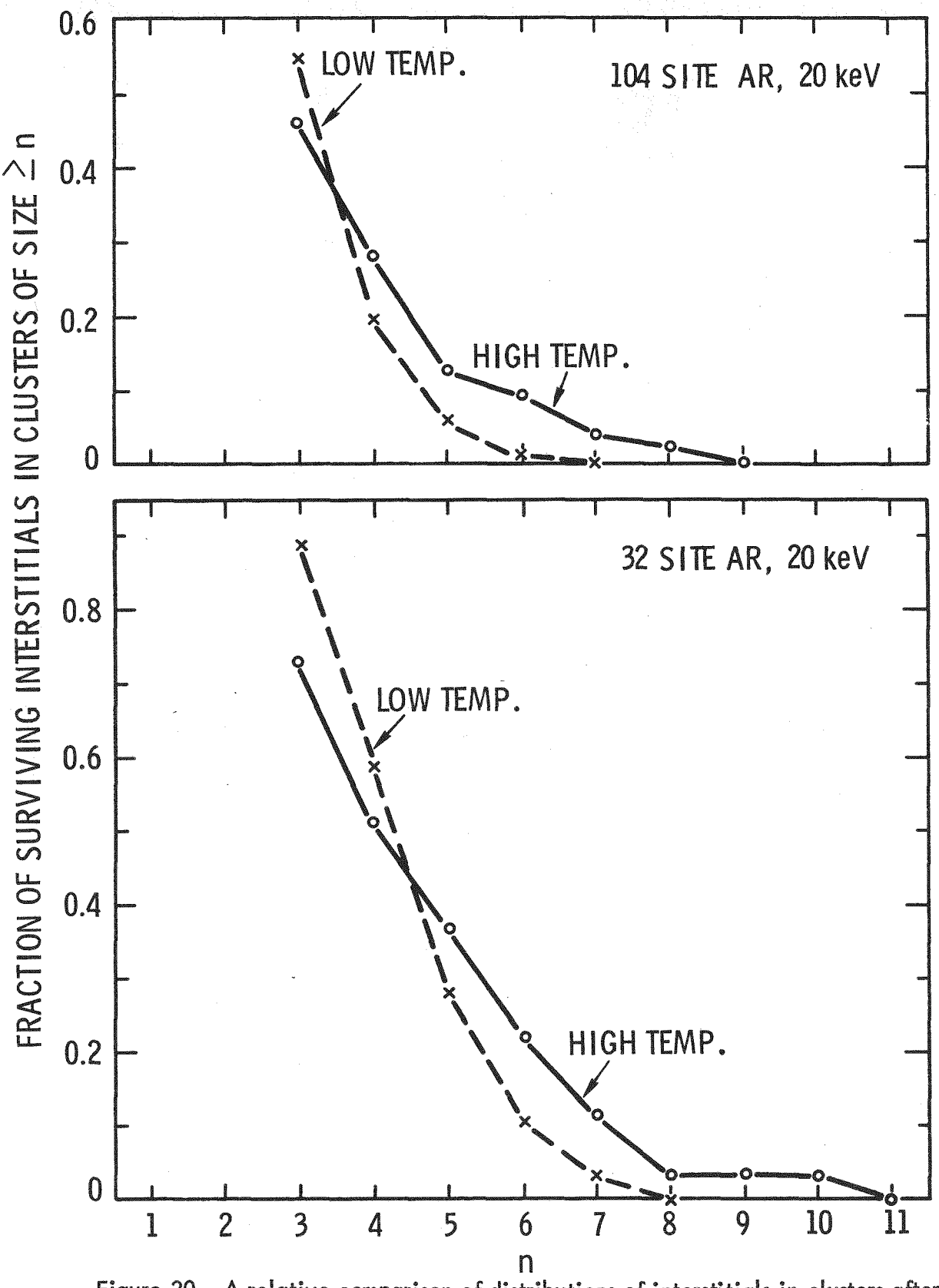


Figure 20. A relative comparison of distributions of interstitials in clusters after high and low temperature anneals. Each integral distribution is normalized to unity.

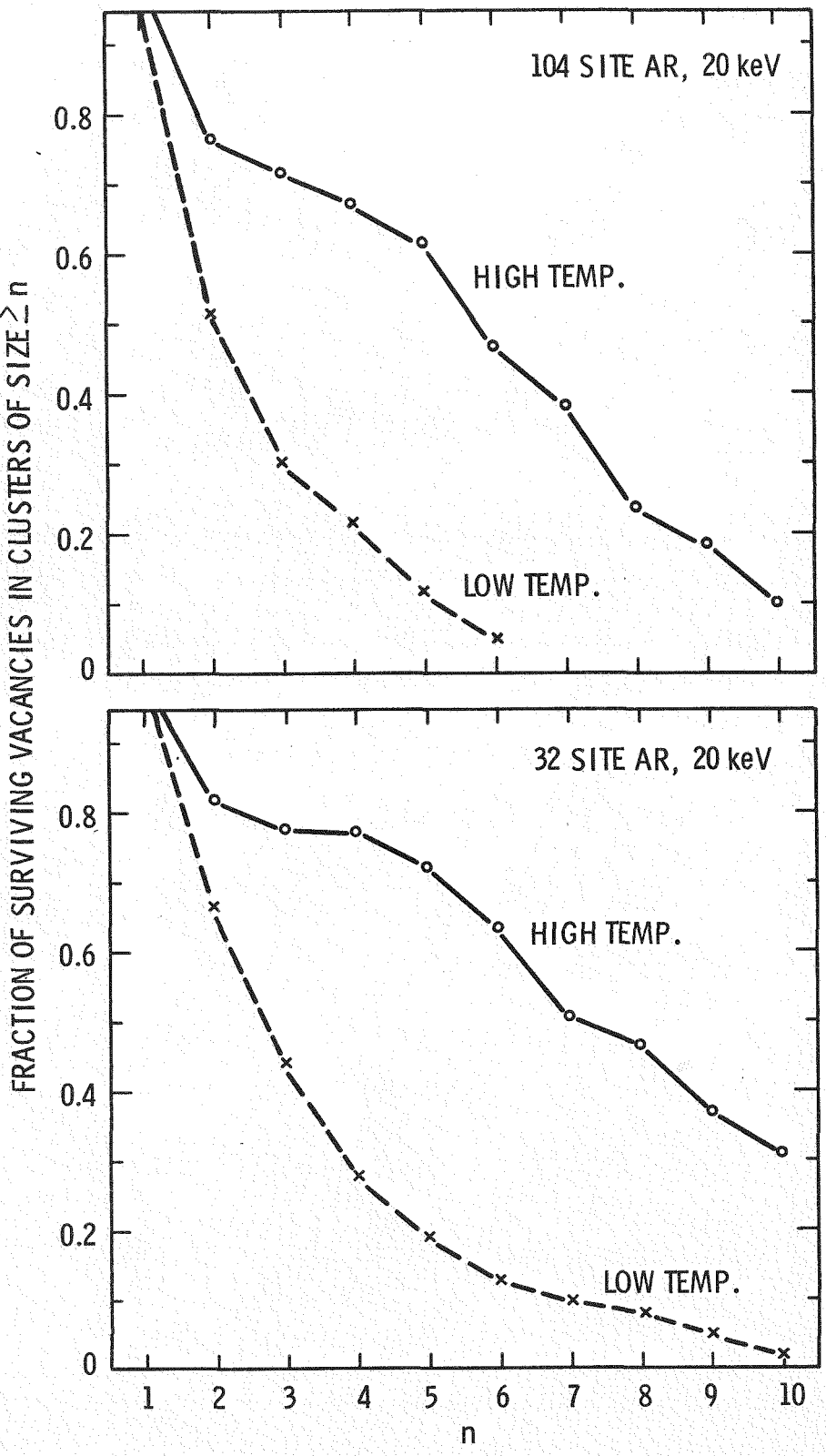


Figure 21. A relative comparison of distributions of vacancies in clusters after high and low temperature anneals. Each integral distribution is normalized to unity.

To distinguish between cluster size distributions and the distribution of defects in clusters, let $N_n^i$ represent the number of interstitial clusters of size n or greater. Then $(N_n^i)_{Hi-T}/(N_n^i)_{Lo-T}$ $<1$ for $n = 3$, $\cong 1$ for $n = 4$, and $>1$ for $n \geq 5$. A similar result holds for vacancy clusters with the crossover point being slightly under $n = 4$. Other comparisons can be made by reference to the tables and figures.

## 5 COMPARISON WITH $\alpha$-IRON (BCC)

In previous work[1] on short-term annealing, a model of $\alpha$-iron (bcc) was used in which a 62 site AR was employed for high temperature runs and a 30 site AR for low temperature runs.

The annihilation characteristics of the $\alpha$-iron data are included in Table 3 for comparison with the present results. It would, of course, be expected that present results obtained with the large AR would be most comparable to the $\alpha$-iron high temperature results and those obtained with the small AR most comparable to the low temperature results. In fact, the effective difference between the 62 site bcc region and the 104 site fcc region is less than suggested by the number of sites involved. The bcc annihilation region is very anisotropic, extending farthest along the close-packed directions (<111>), whereas the fcc annihilation region is more nearly isotropic. Unpublished work by the authors has shown that, in the bcc case, an isotropic region encompassing 112 sites produces annihilation approximately equivalent to the 62 site region. In like manner, the 32 site fcc region was expected to have a smaller effect than the 30 site, markedly anisotropic bcc region.

The similarity in the high temperature annihilation results, after the initial annihilation, is indeed striking and certainly somewhat coincidental considering the numerous differences in the manner in which runs were made in the two cases. The annihilation at low temperature was less in the fcc case (32 site AR) than in the bcc case, as expected.

Some information on the cluster size distributions for $\alpha$-iron is included in Tables 4, 5, 8, and 9. The large AR high temperature $\gamma$-iron results are quite similar to the high temperature $\alpha$-iron results for both interstitials and vacancies. The major difference is the lower production of large vacancy clusters ($\geq$10) by 20 keV cascades in the fcc case. The small AR, low temperature $\gamma$-iron results show considerably less clustering of interstitials than in the $\alpha$-iron case, even though there were fewer interstitials in the latter case. This is presumably because only the $I_1$ was mobile in the former case whereas the $I_2$ was the most mobile defect in the latter case (the $I_1$ was mobile also). For the same reason, vacancy clusters suffered less attrition in the fcc ( $\gamma$-iron) case than in the bcc ( $\alpha$-iron) case at low temperature.

## 6 SUMMARY AND CONCLUSIONS

The displacement cascades simulated by Beeler[2] have been "temperature corrected" (to nominally 300° K and 800° K) by means of a simulated short-term anneal. The annealing model was based on the simulation of $\gamma$-iron by Johnson.[4] Results were obtained with both large (104 sites) and small (32 sites) annihilation regions (AR); the latter is considered the more realistic for the present model.

In the high temperature simulation, it was found that the 104 site AR led to the survival of 2 interstitial-vacancy pairs/keV between 5 and 20 keV; 20-30% of the surviving interstitials and 40-60% of the surviving vacancies were clustered--the other defects migrated away and lost their identification with the cascade. Maximum interstitial cluster sizes were 8 at 20 keV and 5 at 5 keV. The maximum vacancy cluster size was 11 at both energies. The corresponding numbers for the small AR were ~4 defect pairs/keV; 35-50% of the interstitials and 60-70% of the vacancies clustered; and maximum interstitial cluster sizes were 10 and 8 and maximum vacancy cluster sizes were 22 and 12 at 20 and 5 keV, respectively. The number of clusters per cascade increased somewhat faster than the energy for both the large and small AR.

The principal effect of randomizing the spatial distribution of defects in a typical cascade geometry was to diminish vacancy clustering and enhance interstitial clustering somewhat.

In the low temperature simulation, the large AR led to 3.7 defect pairs/keV, and the small AR to 7 pairs/keV. In both cases, clustering of interstitials was more complete than in the high temperature simulation--only 10-14% of the interstitials remained single (and hence mobile)--although maximum cluster sizes (6 in each case) were smaller. The vacancy clusters suffered appreciable attrition causing the cluster size distributions to be shifted strongly toward small sizes.

The high temperature, large AR results are quite similar to those published previously in a simulated annealing of cascades in $\alpha$-iron, but they show a somewhat lower production of large vacancy clusters. The present low temperature results differ from the low temperature $\alpha$-iron results in that fewer interstitial clusters are produced and vacancy cluster attrition is lower in the present case.

## ACKNOWLEDGMENT

This work was supported by the United States Atomic Energy Commission.

## REFERENCES


1. Doran, D. G.: Rad. Effects, 2: 249 (1970).
2. Beeler, Jr., J. R.: Phys. Rev., 150: 470 (1966).
3. Besco, D. G.: General Electric Company Tech. Report GEMP-644, 1967.
4. Johnson, R.A.: Phys. Rev., 145: 423, 152: 629 (1966).
5. Merkle, K. L.: Private Communication.

# DISTRIBUTION FOR HEDL-TME 71-110

## OFFSITE

No. of Copies

216 TID-4500, UC-40

26 AEC Division of Reactor Development and Technology

Director, RDT
Asst. Dir. for Nuclear Safety
Analysis & Evaluation Br, RDT:NS
Asst. Dir. for Plant Engrg, RDT
Facilities Brn, RDT:PE
Components Br, RDT:PE
Instrumentation & Control Br, RDT:PE
Liquid Metal Systems Br, RDT:PE
Asst. Dir. for Program Anal, RDT
Asst. Dir. for Porject Mgmt, RDT
Liquid Metals Projects Br, RDT:PM
FFTF Project Manager, RDT:RE
Asst. Dir. for Reactor Engrg, RDT

No. of Copies

Control Mechanisms Br, RDT:RE
Core Design Br, RDT:RE
Fuel Engineering Br, RDT:RE
Fuel Handling Br, RDT:RE
Reactor Vessels Br, RDT:RE
Coolant Chemistry Br, RDT:RT
Fuel Recycle Br, RDT:RT
Fuels & Materials Br, RDT:RT
Reactor Physics Br, RDT:RE
Special Technology Br, RDT:RT
Asst. Dir. for Engrg Standards, RDT
LMFBR Program Manager, RDT:PM

## ONSITE-HANFORD

No. of Copies

1 RDT Asst Dir for Pacific Northwest Programs

TA Nemzek

1 AEC Richland Operations Office

JM Shivley

WADCO Corporation

EA Evans
TK Bierlein
HR Brager
TT Claudson/JE Irvin
RE Dahl
DG Doran (12)
ER Gilbert
NJ Graves/BL Combs
GL Guthrie
JJ Holmes
JJ Laidler
FJ Leitz

No. of Copies

1 AEC Chicago Patent Group

Richland

14 Battelle-Northwest

Technical Information Files
GL Kulcinski
RA Burnett (12)

WN McElroy
GE Russcher
WF Sheely/JA Christensen
FR Shober
RL Simons
JL Straalsund
ET Weber
HH Yoshikawa
WADCO Document Control
WADCO Tech Pubs